Last Glacial Maximum Climate and Atmospheric Circulation over the Australian Region from Climate Models

Yanxuan DU[1], Josephine R. Brown[1], J. M. Kale Sniderman[1]

[1] School of Geography, Earth and Atmospheric Sciences, University of Melbourne, Parkville, VIC, Australia

5   *Correspondence to*: Yanxuan DU (yanxuand@student.unimelb.edu.au)

Abstract. The Last Glacial Maximum (LGM, ~21,000 years ago) was the most recent time that the Earth experienced global maximum ice volume and minimum eustatic sea level. The regional climate changes over Australia at the LGM remain uncertain. Four Coupled Model Intercomparison Project Phase 6 (CMIP6) models and eight Coupled Model Intercomparison Project Phase 5 (CMIP5) models that were included in the Paleoclimate Modelling Intercomparison Project (PMIP) Phases 3

10   and 4 were used in this research to investigate the temperature, precipitation, and wind changes over Australia at the LGM relative to pre-industrial (PI) and compare the results with existing proxy records and other model studies. The annual multi-model mean (MMM) Australian land surface temperature is estimated to cool by 2.6 °C at the LGM. All models show consistent cooling over the Australian region (0-45°S, 110°E-160°E). The MMM annual precipitation decreased by 0.16 mm/day at the LGM relative to PI over modern Australian mainland areas (10°S-45°S, 110°E-160°E). Precipitation minus

15   evaporation patterns over Australia are also examined to assess the changes in moisture balance at the LGM. Despite reduced LGM precipitation, the greater decrease in LGM evaporation leads to a slightly positive moisture balance in many regions. This is in disagreement with some proxy-based hydroclimate reconstructions of reduced LGM moisture over Australia, which might be due to the interpretations of vegetation-based proxy records or the uncertainties in model representation of moisture fluxes. We find a small equatorward multi-model average displacement of the boundary line

20   between Southern Hemisphere (SH) westerly and easterly winds at the LGM but large model disagreement on a shift in SH mid-latitude westerly winds at the LGM, similar to previous studies.

1 Introduction

The Last Glacial Maximum (LGM, ca. 28-18 thousand years ago (ka)) refers to the coldest interval within the last glacial period. It was a time of global maximum ice volume and associated low eustatic sea-level (Clark et al., 2009). Ice sheets

25   covered large parts of North America, Europe, and Northern Eurasia (Ehlers & Gibbard, 2007). In Australia, Reeves et al. (2013a) present evidence of glaciation in the Snowy Mountains of Southeast Australia and Tasmania, with the most significant glacier advance at around 19.1 ka (Petherick et al., 2013).

Global mean surface air temperature (SAT) estimates during the LGM range from 3.4 to 8.3 °C cooler than pre-industrial based on different model ensemble results constrained with proxy data (Schneider von Deimling et al., 2006;

30   Holden et al., 2010; Annan & Hargreaves, 2013; Tierney et al., 2020a; Seltzer et al., 2021; Annan et al., 2022) with recent

studies suggesting a narrower range of values of 4.5 °C ± 0.9 °C (Annan et al., 2022) and 5.7 °C to 6.5 °C (Tierney et al., 2020a). The global sea level was estimated at ca.120 meters lower than today (Lambeck et al., 2014; Yokoyama et al., 2018), resulting in the expansion of the land areas in many parts of the world, appearance of land bridges and the exposure of Sunda and Sahul shelves in Southeast Asia, which further allowed human migration during this period (Clarkson et al., 2017). The

35 Australian mainland expanded at the LGM, connected by land bridges to New Guinea, Tasmania, and many smaller islands into a single landmass known as "Sahul" (Clarkson et al., 2017, see Figure 1b with the grey shading covering the land areas).
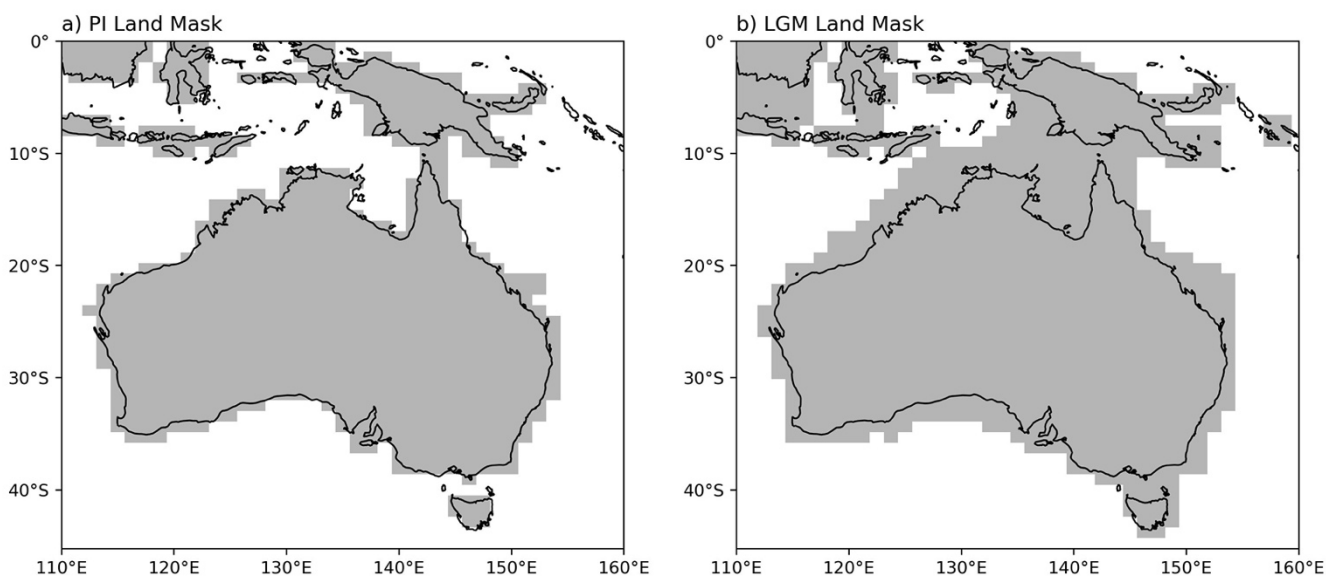
Figure 1: Example of modern day (a) and LGM (b) land masks (shown as grey shading) from CCSM4 model, plotted over modern
40 coastlines.

LGM vegetation was also very different from today. Many regions that are forested today were covered in tundra and grasslands at the LGM (Kageyama et al., 2017). These changes reflect large LGM reduction in terrestrial biomass, related to combinations of lower temperatures, changes in hydroclimate (moisture availability), and/or lower atmospheric

45 CO_2 concentrations (~180 ppm) that cooled the climate and restricted vegetation growth (Scheff et al., 2017; Prentice et al., 2022). Dust suspension and transport was estimated to be more active at the LGM, which was possibly driven by stronger winds and drier climate conditions, particularly in the tropical and high-latitude regions (Lamy et al., 2014; Ujvari et al., 2018), or may have been partly a consequence of the reduced ability of terrestrial vegetation to stabilise soils (Scheff et al., 2017; Roderick et al., 2015).

50 The exact definition of the LGM has varied over time. Traditionally, the concept has denoted the time of maximum global ice volume and/or minimum eustatic sea level, best estimates placing this at ca. 21 ka (Hughes et al., 2013). However, in the Southern Hemisphere (SH), on landmasses remote from continental ice sheets, it has become clear from pollen and

other terrestrial climate proxies that full glacial conditions were maintained in New Zealand and Australia between ca. 28-18 ka (Newnham et al., 2007; Cadd et al., 2021), which Newnham et al. (2007) referred to as the 'extended LGM'. In general,

55   this study will discuss proxy climate records from the period from 28 to 18 ka as broadly representative of LGM climate and compare those records with our model results for temperature, precipitation, and wind patterns over Australia.

     The LGM is commonly recognised as a time of global cooling and lower sea levels, but changes in SH regional temperature, rainfall and atmospheric circulation are less well understood. A limited number of climate modelling studies have focused on conditions during the LGM in the SH (e.g. Rojas et al., 2009; Rojas, 2013), with even fewer studies

60   examining simulations of LGM climate in Australia (e.g. Hope, 2005; Yan et al., 2018). Some studies (e.g. Kageyama et al., 2021; Annan & Hargreaves, 2013; DiNezio & Tierney, 2013; Sime et al., 2013) have begun to explore the new PMIP4 simulations of LGM climate, but there has been little research on the changes in SH climate, including the Australian region in these simulations (or the older PMIP3 ensemble). Therefore, this study aims to investigate the climate (temperature, precipitation, moisture balance and wind) changes at the LGM over the Australian region, making use of available PMIP3

65   and PMIP4 climate model simulations of LGM climate.

1.1 Palaeoenvironmental proxy records for the Australian LGM

In tropical Australasia (see Figure 2 for corresponding region), sea surface temperatures (SSTs) are estimated to have cooled by 1 to 3 °C at the LGM relative to present (Reeves et al., 2013a). The temperature in upland areas in New Guinea is estimated to have reduced by 4 to 6 °C compared to present based on pollen records from the snowlines in the Kosipe Valley

70   (Hope, 2009). A dramatic reduction in tree cover was identified at the LGM in tropical savanna woodland in northern Australia from pollen and geochemical records (Rowe et al., 2021). Rowe et al. (2021) attributed the change in vegetation to a combination of a cooler and drier glacial climate, while also considering the possible role of lower atmospheric CO_2 concentrations and the increased distance of the site from the coastline. Reduced fire activity occurred as a result of less available fuel, indicating that the vegetation at the LGM was less influenced by fire events than today. There is uncertainty

75   about the drivers of LGM climate changes in northern Australia; sparser vegetation has been interpreted previously as a sign of aridity, but it is also likely that low CO_2 played a role in reducing plant biomass (e.g. Scheff et al., 2017; Prentice et al., 2017; Prentice et al., 2022). Moreover, Denniston et al. (2013) found that there is isotopic evidence for LGM moisture as high as today in speleothem records at Ball Gown Cave in tropical northern Australia.

     In temperate Australia during the LGM, a SAT reduction of 4-6 °C has been inferred from pollen records, and SST

80   cooling varying from 3 to 9 °C has been inferred in nearby ocean regions (Petherick et al., 2013). Fossil pollen records indicating widespread reductions in tree cover have often been interpreted as implying drier conditions, i.e. reduced precipitation and/or increased evaporation (Petherick et al., 2013), but the potential role of low atmospheric CO_2 in reducing plant productivity has rarely been considered in the region (Prentice et al., 2017; Sniderman et al., 2019). Moreover, regionally wetter conditions (increased precipitation and/or reduced evaporation) were also present in some parts of the

85   Southern Australian domains (Reeves et al., 2013b), possibly associated with a northward shift of the SH westerlies at the LGM (Kohfeld et al., 2013). Some evidence of higher lake (Lakes Mungo, Keilambete and George) and river levels in the Murray-Darling Basin (Hesse et al., 2018) has been interpreted in terms of greater seasonal runoff due to snowmelt (Petherick et al., 2013), or some combination of higher precipitation and lower evapotranspiration (Hesse et al., 2018). In subtropical eastern Australia, the persistence of moisture-demanding woodlands suggests that the effective precipitation (net

90   moisture) levels did not drop dramatically during the LGM in this region (Cadd et al., 2018).

In the arid interior zone in Australia, the average LGM air temperature was estimated to decrease by 9 °C below present (Miller et al., 1997) based on amino-acid racemisation of emu eggshell. Fitzsimmons et al. (2013) argued that the arid interior experienced extensive dune activity and dust transport, and reduced but episodic fluvial activity at the LGM. However, there is geomorphological evidence for higher lake levels at Lake Frome (Cohen et al., 2015). Evidence of wetter

95   conditions in arid Australia during the LGM was found by Treble et al. (2017) from speleothem records at Mairs Cave, Flinders Ranges in the Southern Australian semi-arid zone. That study suggested that the Flinders Ranges were relatively wet during the LGM, possibly associated with a southward shift of the Intertropical Convergence Zone (ITCZ), allowing more tropical moisture to reach the cave. These proxy records providing evidence of relatively wet conditions at the LGM support the hypothesis proposed by De Deckker et al. (2020), that water was available during the cold and dry LGM period

100   in Australia, sustaining human populations in inland areas.

1.2 Climate models for the LGM

Many previous modelling studies have focused on the LGM. This period is one of the main "entry card" experiments for the Paleoclimate Modelling Intercomparison Project (PMIP) (Kageyama et al., 2017). Some studies have used PMIP simulations with proxy data to reconstruct LGM climate (e.g. Annan & Hargreaves, 2013; DiNezio & Tierney, 2013; Sime et al., 2013).

105   Other studies have compared results from a range of simulations including the LGM as well as historical or future climates (e.g. Chavaillaz et al., 2013; Brown et al., 2020; Liu et al., 2020), using past climates to provide insights into future climate change (Tierney et al., 2020b).

In a recent study, Kageyama et al. (2021) presented global results from PMIP3 and PMIP4 LGM simulations and found that the multi-model global average change in temperature is similar for the two ensembles. The PMIP4 models

110   simulate slightly drier annual precipitation changes in the LGM than the PMIP3 models. Overall, while there are large differences between individual models, the two groups of models are not fundamentally different. In addition, the LGM simulations were found to be broadly consistent with regional proxy reconstructions (Kageyama et al., 2021). In this study, the PMIP3 and PMIP4 LGM simulations are examined in more detail over Australia, considering seasonal anomalies and individual model responses as well as the ensemble mean.

115   The behaviour of the SH westerlies is a major area of research focused on understanding the climate system during the LGM, with relevance for southern Australian climate. Previous modelling studies using coupled atmosphere-ocean models (PMIP2 and 3) and atmosphere-only models (PMIP1) show ambiguous results regarding the latitudinal positions of

the SH mid-latitude westerlies during the LGM. For example, Sime et al. (2013) found strengthening and southward shifts in the maximum 850 hPa SH westerlies based on PMIP2 simulations with an atmosphere-only model (HadAM3). Similarly, a poleward shift in SH surface westerlies was indicated by Kitoh et al. (2001) from an AOGCM used in PMIP1 (MRI-CGCM1 model). However, variations are found between different models, with shifts equatorward (Kim et al., 2003) and no latitudinal change (Otto-Bliesner et al., 2006; Rojas et al., 2009) in SH westerlies also observed from PMIP model simulations. This disagreement across model simulations is consistent with a more recent study (Chavaillaz et al., 2013) using the newer PMIP3 and CMIP5 models, suggesting no agreement was reached between models regarding the latitudinal changes in SH westerlies during the LGM. Rojas (2013) suggested that differences in response may be related to the coupling between atmosphere, ocean and sea ice in the models. Shifts in SH westerlies and influences on Australian climate in CMIP5-PMIP3 and CMIP6-PMIP4 models are investigated in Section 3.2.1 of this paper.

In this paper, the data and methods are described in Section 2, Section 3.1 presents temperature results from models, while wind and precipitation changes at the LGM are shown in Section 3.2 and 3.3, respectively. Relationships between climate variables, such as SH mid-latitude westerly winds and precipitation changes at the LGM in JJA season, and the correlations between seasonal temperature and precipitation patterns are evaluated in Section 3.3.2 as drivers of precipitation change. Section 4 discusses the limitations and consistencies between relevant proxy records and modelling studies, followed by the conclusion in Section 4.4.

2 Data and methods

2.1 Model datasets

This study makes use of PMIP Phase 3 (PMIP3, Braconnot et al., 2012) model simulations which were included in the Coupled Model Intercomparison Project Phase 5 (CMIP5, Taylor et al., 2012), and PMIP Phase 4 (PMIP4, Kageyama et al., 2018) simulations which were included in CMIP Phase 6 (CMIP6, Eyring et al., 2016). Datasets from eight CMIP5 models and four CMIP6 models that were included in PMIP3 and PMIP4 were analysed, based on data availability via the Earth System Grid Federation (the set of models is therefore smaller than Kageyama et al. 2021, who made use of some models only available in PMIP databases). See Table 1 for list of models with LGM simulations included in this study. It was decided not to include CESM2-WACCM-FV2 model (Danabasoglu et al., 2020), which also performed LGM simulations due to an unrealistic climate sensitivity found by Zhu et al. (2021). Large global LGM cooling was simulated in the model, which is not consistent with proxy records and other model simulations in this study, biasing the MMM temperature results. PMIP3/CMIP5 and PMIP4/CMIP6 models shown in Table 1 are referred to as CMIP5 and CMIP6 models hereafter for simplification.

Table 1: List of models with models included in the study, model reference and PMIP/CMIP generation.

Model name	Reference	PMIP/CMIP generation
AWI-ESM-1-1-LR	Sidorenko et al. (2015), Lohmann et al. (2020)	PMIP4/CMIP6
CCSM4	Brady et al. (2013)	PMIP3/CMIP5
CNRM-CM5	Voldoire et al. (2013)	PMIP3/CMIP5
FGOALS-g2	Zheng and Yu (2013)	PMIP3/CMIP5
GISS-E2-R	Ullman et al. (2014)	PMIP3/CMIP5
INM-CM4-8	Volodin et al. (2018)	PMIP4/CMIP6
IPSL-CM5A-LR	Dufresne et al. (2013)	PMIP3/CMIP5
MIROC-ES2L	Ohgaito et al. (2021), Hajima et al. (2020)	PMIP4/CMIP6
MIROC-ESM	Sueyoshi et al. (2013)	PMIP3/CMIP5
MPI-ESM-P	Adloff et al. (2018)	PMIP3/CMIP5
MPI-ESM1-2-LR	Mauritsen et al. (2019)	PMIP4/CMIP6
MRI-CGCM3	Yukimoto et al. (2015)	PMIP3/CMIP5

150

The models in CMIP6 include some modifications and improvements relative to the older CMIP5 generation (Eyring et al., 2016). There are also some minor differences in the LGM experiment boundary conditions for the CMIP5 (PMIP3) and CMIP6 (PMIP4) experiments. Compared to PMIP3 experiments, new and updated boundary conditions were included in PMIP4 (as shown in Table 2), enabling the systematic analysis of the vegetation and dust forcing effects. Further,
155   the PMIP4 simulations highlight the specification of ice sheets, with three distinct ice sheet reconstructions available, allowing assessments of the impacts from uncertainties in ice-sheet reconstructions or boundary conditions (Kageyama et al., 2017).

160

Table 2: Summary of the main forcing or boundary conditions (experimental design) for the LGM simulations in PMIP3 and PMIP4
165 models (PMIP4 from Table 1 in Kageyama et al. (2017); PMIP3 from PMIP3 website: https://pmip3.lsce.ipsl.fr/). Some boundary
conditions are set as the same as pre-industrial control (piControl) values.

Forcing or Boundary conditions	PMIP4 LGM value	PMIP3 LGM value
Atmospheric trace gases	CO_2 = 190 ppm CH_4 = 375 ppb N_2O = 200 ppb CFC = 0 O_3 = same as in CMIP6 *piControl*	CO_2 = 185 ppm CH_4 = 350 ppb N_2O = 200 ppb CFC = 0 O_3 = same as in CMIP5 *piControl*
Insolation	eccentricity: 0.018994 obliquity: 22.949° perihelion – 180° = 114.42°	eccentricity: 0.018994 obliquity: 22.949° perihelion – 180° = 114.42°
Ice sheets (components of model modified to represent influence of LGM ice sheet)	coastlines bathymetry ice-sheet extent altitude rivers	land-sea mask land surface elevation ocean bathymetry
Vegetation	Unless a model includes dynamic vegetation or interactive dust, the vegetation should be prescribed to be the same as in the DECK and historical runs (CMIP6 *piControl*)	as in *piControl*
Dust	as in *piControl* or *lgm* (three options)	as in *piControl*

For this research, monthly surface temperature (ts), surface air temperature (tas), precipitation (pr),
evapotranspiration (evspsbl) and 850 hPa wind (ua and va at 850 hPa) data from each model for a model pre-industrial
170 control ('piControl') and LGM ('lgm') simulations were analysed. All data was regridded using first-order conservative
remapping onto a 1.5° × 1.5° longitude-latitude grid. Both zonal (u) and meridional (v) components of the wind were
analysed, at 850 hPa except for CMIP6 INM-CM4-8 model, which only provided only near-surface (10 metre) wind data for
LGM simulations.

2.2 Run Length and Control Simulation

175   The LGM simulations are compared with pre-industrial (PI) climate as the control or baseline, similarly to many previous studies (e.g. Kageyama et al., 2021). Pre-industrial ("piControl") experiments are simulations with atmospheric composition and other boundary conditions prescribed and held constant at values representing climate before industrialisation, i.e. reference year 1850 (Eyring et al., 2016). The LGM simulations from different models run for different numbers of years with a minimum length of 100 years, therefore, it is necessary to determine a uniform length of time that captures the

180   average climatology for each model simulation to assess changes in climate variables. In this research, the first 100 years of output from each model was selected and averaged in order to represent the mean state of PI and LGM climate conditions.

2.3 Classification of Australian Regions

Different regions of Australia experience different climate regimes in the present day, and are likely to respond differently to LGM climate forcing. Each region also experiences greater seasonal precipitation at a different time of year, with the north

185   receiving most precipitation in summer and the south in winter. We therefore divide Australia into three main regions in order to examine the LGM climate response in detail at seasonal time scales.

        Shown in Figure 2, the Australian region is defined in this research bounded by longitudes from 110°E to 160°E, latitudes from 0 to 45°S. The Northern Australasia domain in the spatial plots is defined longitudes from 110°E to 160° E, and latitudes from 0 to 20°S (including New Guinea and parts of Indonesia); the Southern Australia domain is defined by

190   longitudes from 110°E to 160°E, and latitudes from 20°S to 45°S. Lastly, the Central Australian domain is shown in the spatial plots bounded by 20°S to 35°S and 120°E to 145°E. These three domains broadly correspond to the Tropical Australasia, Temperate Australia and Arid Interior regions discussed in Section 1.1.

195

200
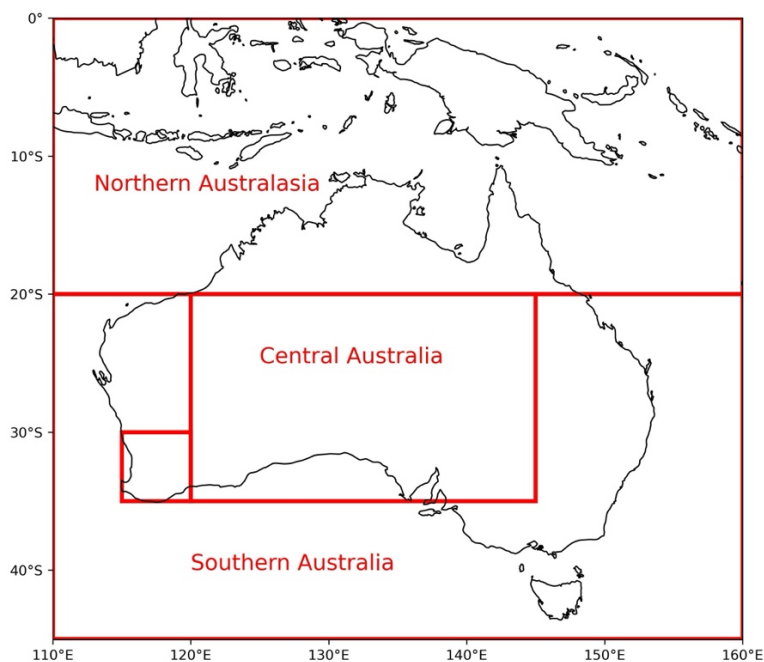
205

Figure 2: Classification of Northern Australasia, Central, and Southern Australia domains shown by red rectangles with modern day coastlines. The Central Australia domain is a subset of the larger Southern Australia domain. The south-west box for detecting JJA frontal precipitation that is most sensitive to westerlies is also indicated in the Southern Australia domain.

3 Results

210   ### 3.1 Surface temperature

In this Section, the changes in surface temperature (ts) in the LGM model simulations are evaluated in comparison with PI simulations. Figure 3 shows the simulated temperature patterns from CMIP5 and CMIP6 model ensembles, the LGM temperature over Australia is warmer in the CMIP6 simulations than in the CMIP5 simulations. This differs from Kageyama et al. (2021), where most of the Australian interior is slightly cooler in PMIP4 than PMIP3 LGM simulations, possibly due to

215   the slightly different sets of models used. Despite some differences between the CMIP6 and CMIP5 model simulations in LGM temperature over Australia, we combine the four models from CMIP6 and the eight models from CMIP5 together into a large ensemble of models, for assessing the multi-model mean (MMM) change in temperature patterns at the LGM in this section.
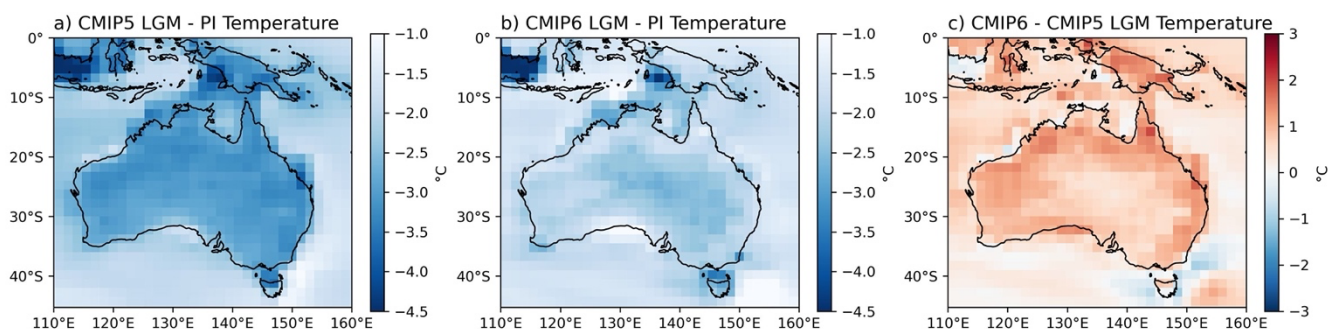
Figure 3: (a) LGM - PI mean annual surface temperature (in °C) simulated by the ensemble of CMIP5 models, (b) LGM – PI mean annual surface temperature anomaly (in °C) simulated by CMIP6 models, (c) difference between the CMIP6 and CMIP5 LGM ensembles (in °C) over Australian region.

225   To explore the extent of model agreement on LGM temperature, Figure 4 shows the mean annual LGM surface temperature changes over Australia in individual CMIP5 and CMIP6 models. All models agree on the sign of temperature change over the Australian region, with mean annual cooling during the LGM. The cooling patterns are overall similar across most models, with more cooling over Northern Australia and the Maritime Continent, and more cooling over land than ocean. CMIP5 FGOALS-g2 model simulates the strongest LGM land cooling over Australia, with an average

230   temperature anomaly of -4.0 °C, compared to the MMM land average of -2.6 °C (see Table 3). The model differences between CMIP6 models are much smaller than between CMIP5 models, possibly due to model improvements or the smaller set of models.
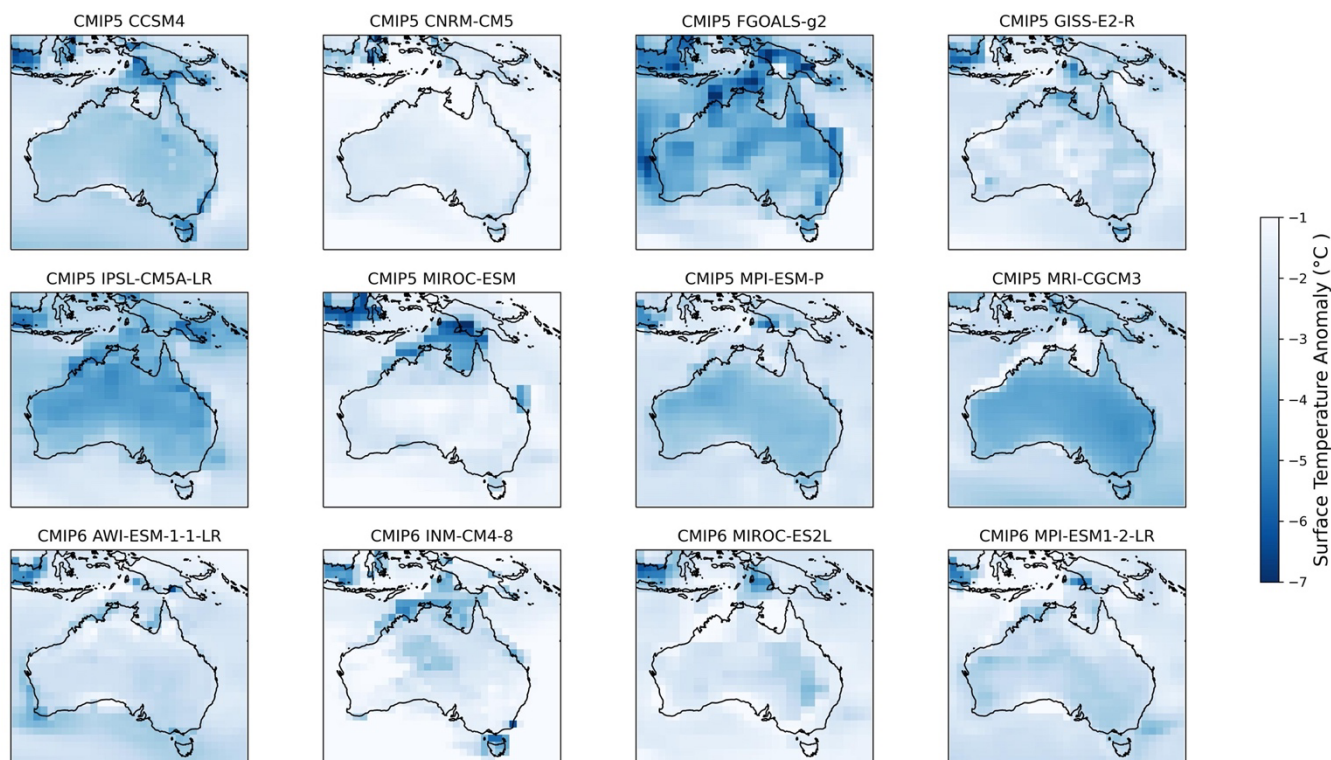
Figure 4: LGM - PI mean annual surface temperature anomaly (°C) simulated by individual CMIP5 and CMIP6 models over Australian region.

The MMM seasonal variations in surface temperature changes at the LGM over Australia are shown in Figure 5. The austral winter JJA season shows the strongest land average cooling (-2.9 °C, refer to Table 3) at the LGM, mostly occurring along the modern coastlines in the northern and temperate Australian regions. There is more cooling over land in DJF and SON compared to JJA and MAM. The warm anomalies in DJF and SON may be due to the extension of land areas at the LGM due to lower sea level, where land areas warm more than surrounding oceans during these seasons. A similar response may also explain the coastal cooling anomalies in JJA and MAM when land cools more than ocean in these colder seasons.

Moreover, orbitally-driven changes in top of the atmosphere insolation during the LGM (see Kageyama et al., 2017) may also play a role in the seasonal differences shown in Figure 5. For the latitude range where Australia is located (~10°S to 45°S), there is an increase in insolation from January to June of 1 to 2 W/m^2 and a decrease in insolation from August to December of up to 4 W/m^2. This means that there should be a slightly enhanced cooling in August to December (particularly influencing Spring, SON) and a slightly reduced cooling in January to June (particularly MAM) relative to the average LGM cooling response. The anomalies may nearly cancel for JJA and DJF depending on the latitude.
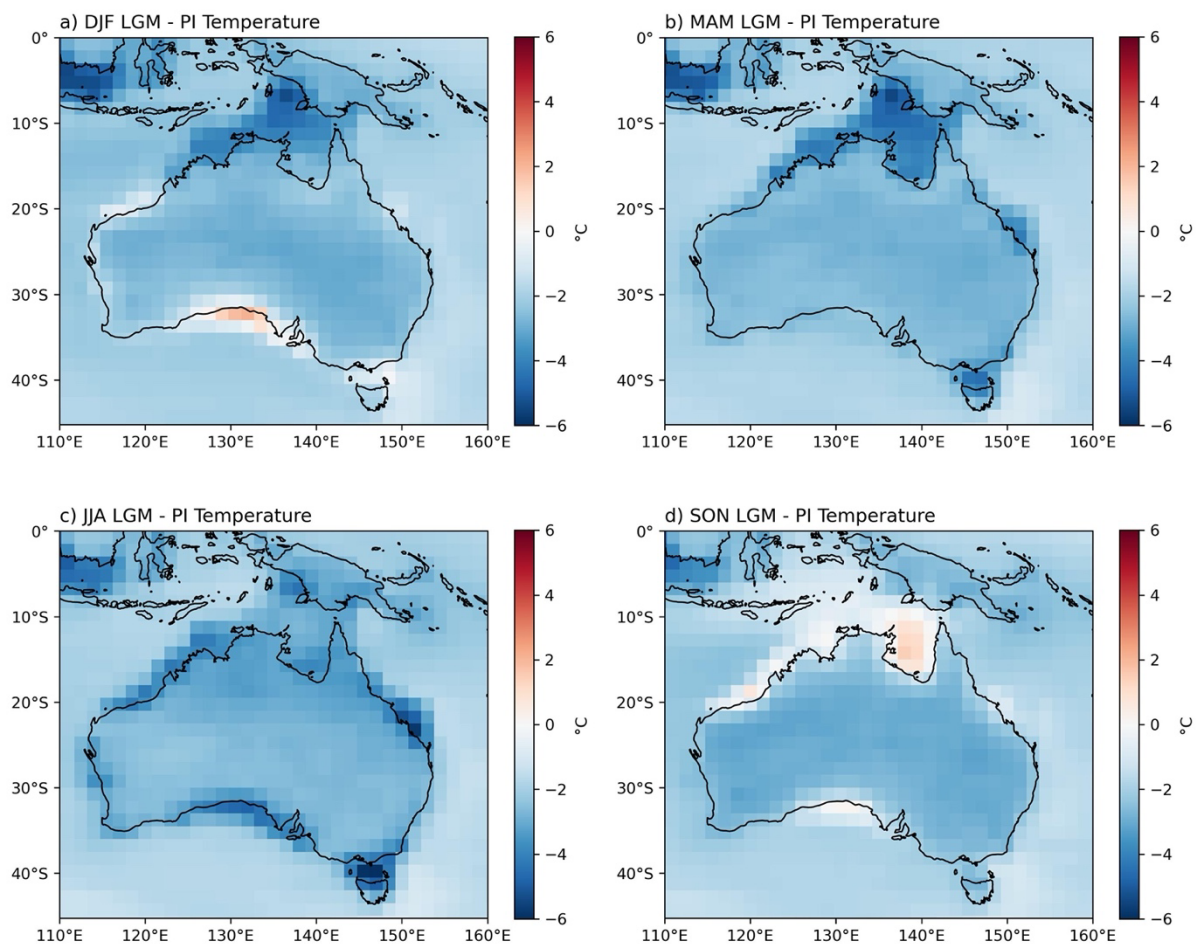
Figure 5: MMM seasonal anomalies for LGM - PI surface temperatures (°C) simulated by the ensemble of CMIP5 and CMIP6 models for
(a) DJF, (b) MAM, (c) JJA and (d) SON seasons over Australian region.

255

260

Table 3: Average land surface temperature anomalies (°C) for annual mean, DJF and JJA seasons over Australia (land areas within
265   domain 0-45°S, 110°E-160°E) for each CMIP5 and CMIP6 models and the multi-model mean (MMM).

Model name	Annual average (°C)	DJF average (°C)	JJA average (°C)
AWI-ESM-1-1-LR	-2.2	-1.6	-3.1
CCSM4	-3.1	-3.2	-3.2
CNRM-CM5	-1.8	-1.5	-2.1
FGOALS-g2	-4.0	-3.3	-4.5
GISS-E2-R	-2.4	-2.6	-2.4
INM-CM4-8	-1.9	-1.7	-2.1
IPSL-CM5A-LR	-3.9	-4.1	-3.9
MIROC-ES2L	-2.0	-1.8	-2.1
MIROC-ESM	-2.0	-1.8	-2.3
MPI-ESM-P	-3.2	-3.3	-3.1
MPI-ESM1-2-LR	-2.4	-2.3	-2.6
MRI-CGCM3	-3.7	-3.8	-3.9
MMM	-2.7	-2.6	-2.9

3.2 Winds

3.2.1 Shifts of the westerlies

We are interested in investigating the meridional displacement of the SH mid-latitude westerly winds at the LGM,
270   in comparison with previous studies (see Section 1.2), as these winds play an important role in the climate of southern
Australia (e.g. Hope et al., 2010). There is large model disagreement over changes in the westerlies in both JJA
(Supplementary Figure S1) and Annual (not shown) in the Australian region and also at a hemispheric and global scale (not
shown). Some models show weakening and other models show strengthening in the region to the south of Australia, with
little change in the MMM. To further investigate shifts in the extent of SH westerly winds or changes in their intensity, the
275   zonal-mean zonal wind is plotted over the SH tropics and midlatitudes. Figure 6 shows the zonal-mean 850 hPa zonal winds
in JJA over SH (0-70ºS).

The majority of models do not show clear evidence of latitudinal changes for maximum mid-latitude zonal wind
speed at the LGM compared to PI, and there are some disagreements between models (see Figure 6). There is a weak
equatorward shift in maximum zonal wind speed seen in IPSL-CM5A-LR and MIROC-ESM models. However, there also

280   seems to be opposite poleward shifts of the maximum zonal winds in CCSM4, FGOALS-g2 and MRI-CGCM3 models. Most models except CCSM4 and MRI-CGCM3 models show overall weakening of SH mid-latitude westerlies at the LGM compared to PI.

        The latitudinal positions of the boundary lines between SH westerlies and easterlies (i.e. latitude of zero zonal wind) for each CMIP5 and CMIP6 model in JJA season for both PI and LGM simulations are also calculated over the Australian

285   domain (110ºE to 160ºE), values are given in Table 4. All models except FGOALS-g2 model show a positive (equatorward) shift for the boundary lines at the LGM relative to PI, even for the models with poleward shifted maximum zonal winds (e.g. CCSM4 and MRI-CGCM3, as stated earlier). CMIP5 FGOALS-g2 model simulated a poleward (negative) shift in both the latitudinal positions for the boundary lines and its SH maximum zonal winds. The two models that simulated relatively large displacement of boundary lines (CNRM-CM5, GISS-E2-R models) show no change in their maximum zonal winds (see

290   Figure 6).
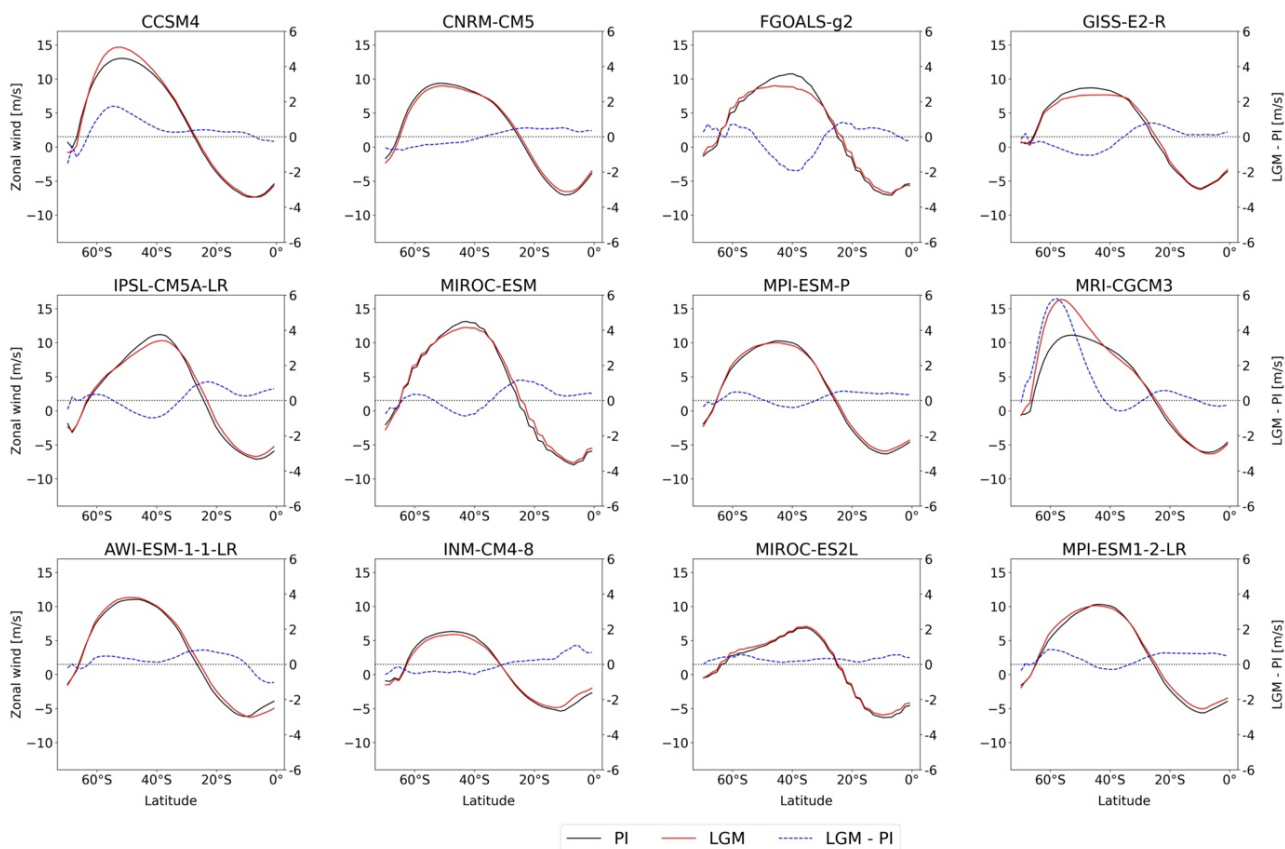
Figure 6: JJA Zonal-mean zonal wind (m/s) at 850 hPa simulated by individual CMIP5 and CMIP6 models (except INM model which provided only near-surface winds) for SH (0 to 70ºS). PI in black colour and LGM in red colour, blue dashed line is LGM anomalies (LGM - PI). The LGM - PI zonal wind anomaly (m/s) for each model is displayed on a secondary y-axis. Zonal mean is calculated over all longitudes.

Table 4: Latitudes of zero westerly wind speed (westerly-easterly boundary) for each CMIP5 and CMIP6 model in JJA season (INM-CM4-8 model used near-surface winds). Calculations were over the Australian domains from 110ºE to 160ºE.

Model name	PI (º)	LGM (º)	LGM – PI (º)
AWI-ESM-1-1-LR	-24.52	-23.46	1.06
CCSM4	-25.58	-25.09	0.49
CNRM-CM5	-23.24	-22.18	1.06
FGOALS-g2	-21.15	-22.41	-1.26
GISS-E2-R	-23.76	-22.43	1.33
INM-CM4-8	-28.97	-28.86	0.11
IPSL-CM5A-LR	-22.71	-21.60	1.11
MIROC-ES2L	-23.34	-23.02	0.32
MIROC-ESM	-24.16	-22.95	1.21
MPI-ESM-P	-23.94	-23.29	0.66
MPI-ESM1-2-LR	-23.46	-22.65	0.81
MRI-CGCM3	-23.00	-22.09	0.91
MMM	-23.99	-23.34	0.65

300

3.3 Precipitation

In the present-day climate, regional precipitation variations over Australia are associated with seasonal variations in atmospheric circulation. Austral summer (DJF season) is the period when the Indo-Australian summer monsoon is most active, bringing precipitation to northern Australia and nearby Maritime Continent areas. In austral winter (JJA season), the

305 SH westerlies shift equatorward, bringing rainfall to the southern Australian region. The LGM changes in precipitation over the Australian region are therefore discussed with a focus on seasonal anomalies.

The LGM - PI annual average precipitation anomalies for each model over Australia are shown in Figure 7. It is evident from Figure 7 that the largest model precipitation anomalies occur over northern Australia and the Maritime Continent, due to the higher absolute precipitation totals in the tropics. Larger model disagreement over northern Australia

310 may be due to the different changes in SST and atmospheric circulations simulated in each model in this region, where model precipitation is highly sensitive to SST gradients (e.g. Chadwick et al., 2013). Some models (e.g. GISS-E2-R and INM-CM4-8) simulate increased precipitation in the tropical monsoon region whereas most of the other models show drier conditions. Most models agree on an annual mean decreased precipitation at the LGM averaged over the Australia mainland,

however, regional increases in precipitation are also simulated by most models. Individual precipitation changes in the DJF
315 and JJA season are shown in Supplementary Figures S2 and S3.
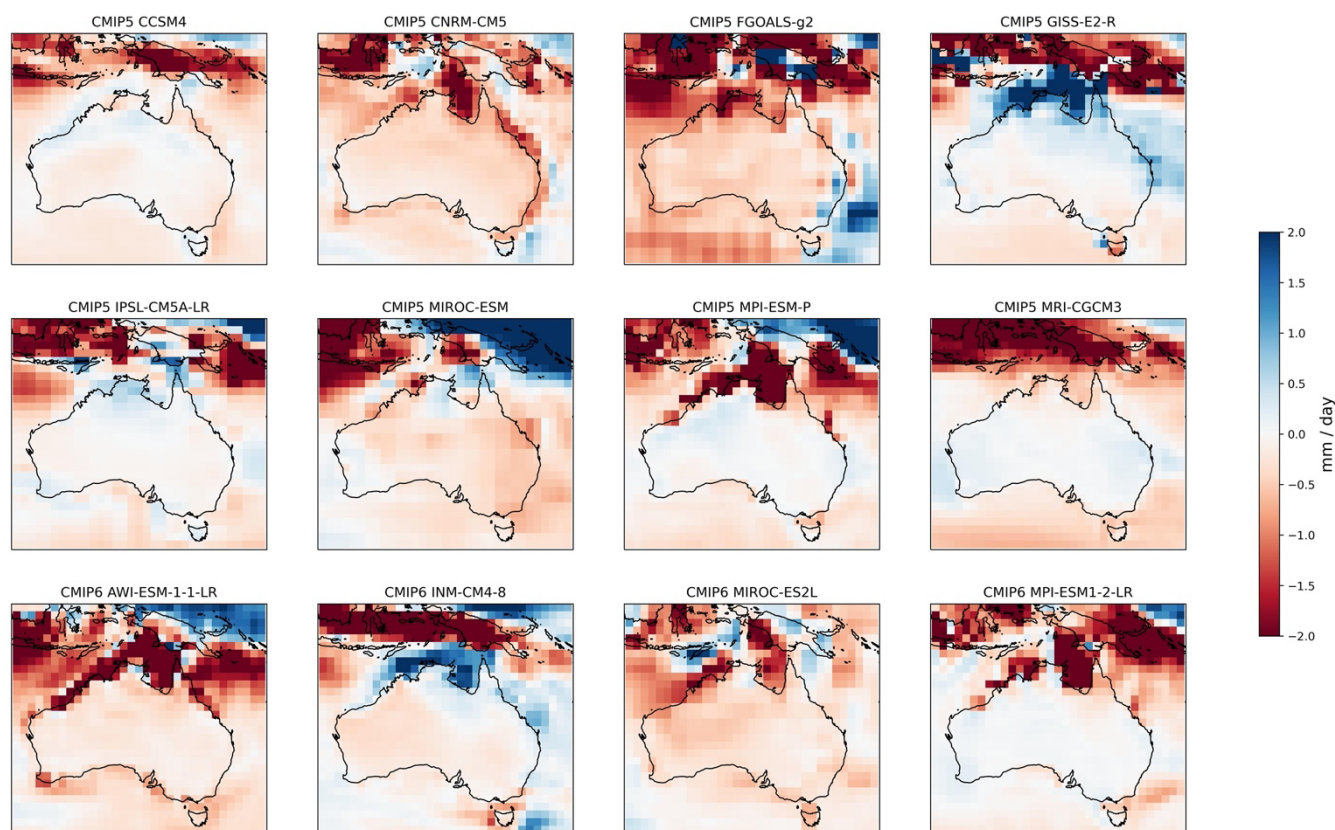
Figure 7: LGM – PI mean annual precipitation anomaly (mm/day) simulated by individual CMIP5 and CMIP6 models over the Australian domains.

320

MMM seasonal precipitation anomalies from the combined CMIP5 and CMIP6 model ensemble at the LGM over
Australia are shown in Figure 8 and seasonal precipitation changes over specific domains are summarised in Table 5
(seasonal precipitation comparisons between CMIP5 and CMIP6 models is presented in Supplementary Figure S4). Austral
winter (JJA) season shows the strongest area-average land drying (-0.59 mm/day) over Australia (0-45°S, 110°E-160°E)
325 during the LGM, dominated by the strong precipitation reduction over northern Australia and the Maritime Continent,
consistent with previous analysis of PMIP3 LGM simulations (Yan et al., 2018). The south-western corner of Australia
shows an average increase in precipitation in JJA (Figure 8c). In austral summer (DJF) season, an increase in precipitation
can be seen over parts of northern Australasia, particularly the central "Top End" region, while other regions become drier
(Figure 8a). Yan et al. (2018) identified increased Australian monsoon precipitation in early austral summer (November-

330   December) in PMIP3 LGM simulations, however we do not find a clear increase in DJF based on the models examined here. Most parts of Australia become drier in MAM, whereas there is a strong increase in precipitation in the tropical north-west (including over the Sahul shelf) and along the east coast in SON.
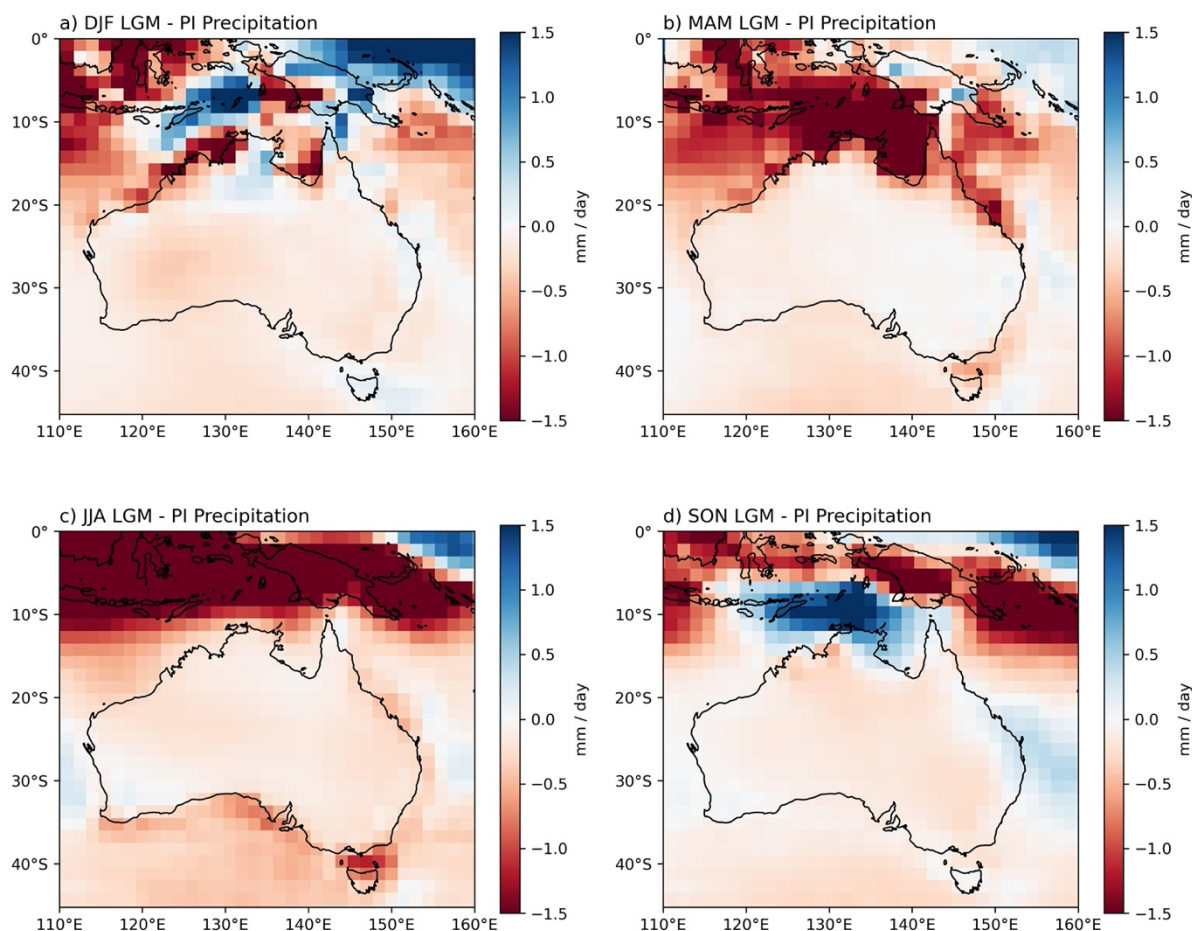
335   **Figure 8:** MMM seasonal anomalies for LGM – PI precipitation (mm/day) simulated by the ensemble of CMIP5 and CMIP6 models for (a) DJF, (b) MAM, (c) JJA and (d) SON seasons over Australian region.

3.3.1 Precipitation minus evapotranspiration (P-E)

As some proxy records provide information about available moisture or effective precipitation changes at the LGM relative

340   to PI, instead of direct evidence for precipitation changes (e.g. Petherick et al., 2013; Sniderman et al., 2019; Fitzsimmons et al., 2012), we also examine changes in the moisture balance or P-E (precipitation minus evapotranspiration) in the LGM

simulations. Cooler conditions at the LGM may lead to reduced evaporation and hence a positive P-E despite reduced precipitation (e.g. Scheff et al., 2017; Kageyama et al., 2021).

345 Annual mean LGM precipitation and evapotranspiration changes over the Australian regions are shown in Figure 9a and 9b while net precipitation (P-E) is shown in Figure 9c. There is an annual mean reduction in precipitation during the LGM across the Australian mainland, New Guinea and parts of the Maritime Continent, with an annual average land precipitation change of -0.3 mm/day (based on PI land mask, so excluding coastal areas which are land in the LGM only). The strong precipitation reductions simulated in the expanded land areas in the northern tropical Australasia monsoon region and the exposed Bass Strait region are associated with decreased evaporation rates at the LGM, so that overall increased 350 LGM P-E was simulated (Figure 9). Changes in both precipitation and P-E averaged over different land domains are given in Table 5.
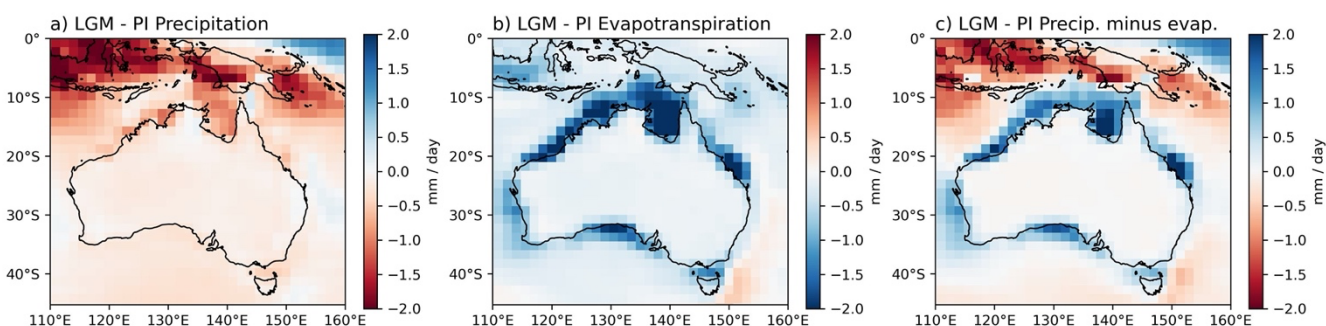
Figure 9: LGM – PI mean annual (a) precipitation (b) evapotranspiration and (b) P-E (in mm/day) simulated by the ensemble of CMIP5
355 and CMIP6 models over Australian region.

Figure 10 shows the LGM seasonal variations in net precipitation (P-E) over Australia, which can be compared with the seasonal changes in precipitation shown in Figure 8. In comparison to the variable precipitation pattern at the LGM (Figure 8), the P-E pattern (Figure 10) provides more seasonally consistent spatial changes over Australia during the LGM
360 with the largest increase in P-E over the expanded land areas at the LGM.
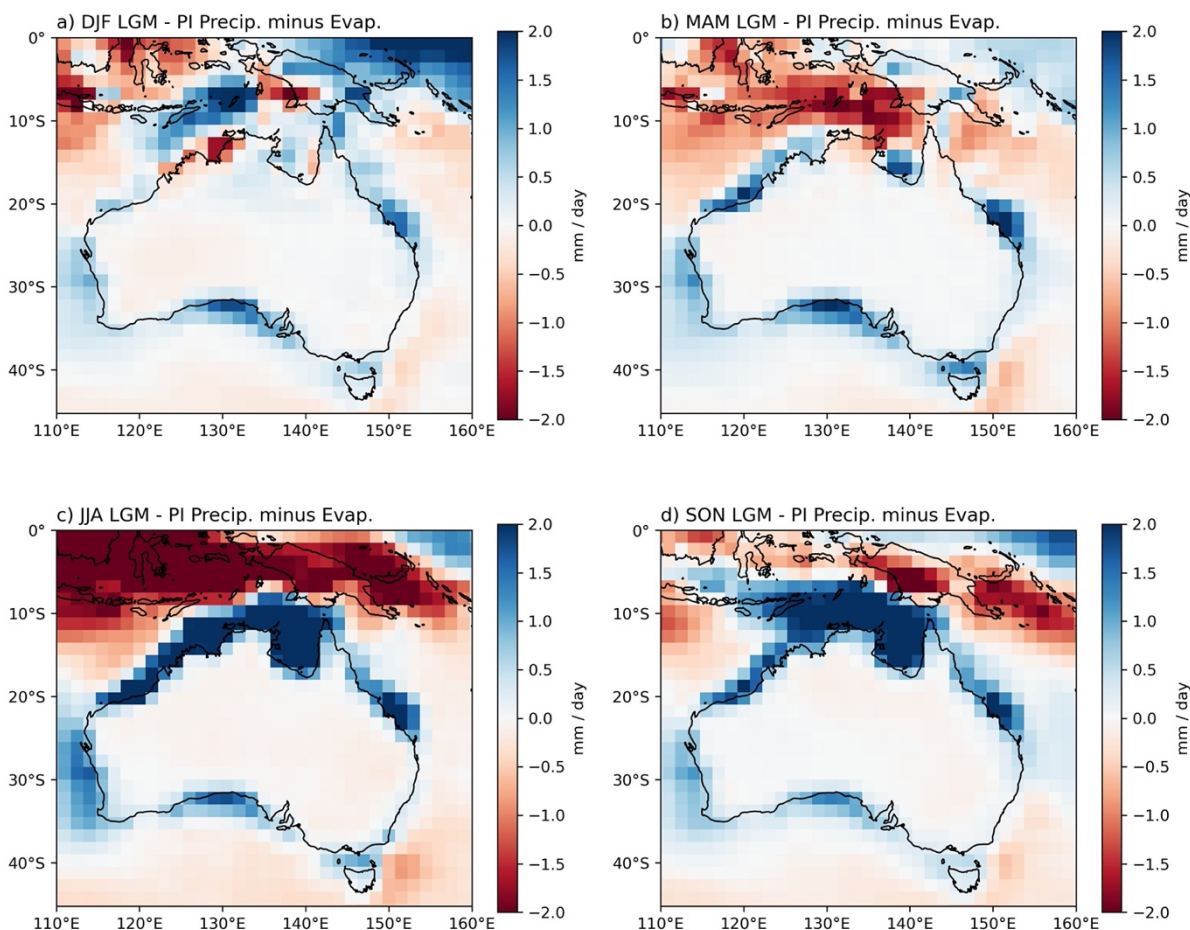
Figure 10: MMM seasonal anomalies for LGM – PI precipitation-evapotranspiration (P-E, mm/day) simulated by the ensemble of CMIP5 and CMIP6 models for (a) DJF, (b) MAM, (c) JJA and (d) SON seasons over Australian region. This can be compared with MMM seasonal precipitation shown in Figure 5 and MMM seasonal evapotranspiration shown in Supplementary Figure S4.

Table 5 shows the average land precipitation and P-E changes at the LGM in individual models over northern (0-20°S, 110°E-160°E) in DJF season and southern Australia (20°S-45°S, 110°E-160°E; see Figure 2) in JJA season and the annual mean anomalies over the whole domain. The Australian mainland region experienced an increase in P-E simulated in all models, with a MMM P-E increase of 0.14 mm/day (Table 5). Individual model simulations of LGM P-E changes can be seen in Supplementary Figure S5.

In the Northern Australasia domain, most models show consistent DJF drier conditions in both average LGM precipitation and P-E changes, although large model disagreements occur (see DJF P-E changes in individual models in Supplementary Figure S6). All models except GISS-E2-R simulated more positive P-E anomalies compared to the corresponding LGM precipitation change. In the Southern Australia region, all models agree on reduced JJA area-average precipitation (see individual model simulations in Supplementary Figure S3) and positive P-E anomalies at the LGM, with

the exception of 'FGOALS-g2' model that very small negative JJA P-E anomaly (-0.05 mm/day) was simulated (Table 5). Mean P-E changes at the LGM in JJA season for each model over the Australian domain are shown in Supplementary Figure S7.

380

Table 5: Average land precipitation and P-E LGM anomalies (mm/day) over Northern Australasia (0-20°S, 110°E-160°E) in DJF season. JJA land averages over Southern Australia (20°S-45°S, 110°E-160°E). Annual mean land average changes for modern Australia mainland (10°S-45°S, 110°E-160°E) for each CMIP5 and CMIP6 model and MMM. Land is defined by PI land mask.

Model name	DJF average over Northern Australasia land (mm/day)		JJA average over Southern Australia land (mm/day)		Annual average over modern Australia mainland (mm/day)	
	Precipitation	P - E	Precipitation	P - E	Precipitation	P - E
AWI-ESM-1-1-LR	-0.85	-0.64	-0.25	0.06	-0.38	0.00
CCSM4	-0.48	-0.24	-0.20	0.03	-0.06	0.18
CNRM-CM5	-0.63	-0.12	-0.15	0.19	-0.38	0.10
FGOALS-g2	-0.58	-0.14	-0.70	-0.05	-0.44	0.04
GISS-E2-R	1.02	0.70	-0.14	0.06	0.18	0.31
INM-CM4-8	-0.19	0.18	-0.07	0.21	-0.06	0.22
IPSL-CM5A-LR	1.10	1.17	-0.19	0.10	0.04	0.28
MIROC-ES2L	-0.85	-0.39	-0.19	0.11	-0.37	0.05
MIROC-ESM	0.53	0.74	-0.26	0.10	-0.27	0.11
MPI-ESM-P	-0.83	-0.20	-0.03	0.10	-0.12	0.05
MPI-ESM1-2-LR	-0.61	-0.25	-0.03	0.11	-0.08	0.08
MRI-CGCM3	-1.23	-0.86	-0.04	0.25	0.00	0.30
MMM	-0.30	-0.01	-0.19	0.11	-0.16	0.14

385 ### 3.3.2 Drivers of precipitation change

3.3.2.1 Temperature

LGM cooling is likely to lead to overall drier conditions due to the thermodynamic response (a colder atmosphere holds less moisture), as seen in the annual mean MMM change (Figure 4). However, the models do not simulate drying over all regions

or in all seasons over Australia. For instance, annually wetter conditions are found over the south-west Australia in some
390   models (Figure 7).

The relationships between temperature and precipitation changes at the LGM compared to PI are evaluated over the
monsoon-affected Northern Australasia domain in this section as temperature and precipitation patterns may be closely
related in the tropics (e.g. Chadwick et al., 2013). Figure 5 shows the MMM seasonal changes for surface temperature and
Figure 8 shows the MMM seasonal changes for precipitation during the LGM. Wetter conditions are found to the north of
395   Australia in SON and DJF (Figure 8), possibly in response to changes in seasonal heating over the exposed continental shelf
or changes in atmospheric circulation.

The cooling anomalies over Northern Australasia in MAM season (Figure 5b) appear to correspond tothe strong
drying anomalies in the same region (Figure 8b). However, the opposite relationship can also be seen. In DJF season, both
increased and decreased precipitation is simulated over Northern Australasia (Figure 8a), however, reduction in temperature
400   is seen across the whole region (Figure 5a). Similarly, warming anomalies are found over the central southern coastlines in
DJF and SON (Figure 5a, d), while no large changes in precipitation are seen over the same region (Figure 8a, d). Thus,
there is no simple linear relationship between regional patterns of LGM temperature and precipitation change.

3.3.2.1 Winds

We now investigate the drivers of LGM precipitation patterns in southern Australia by examining the correlation between
405   precipitation in the south-west of Australia and SH mid-latitude westerlies in JJA, since they shift equatorward in this
season, bringing moisture mainly via frontal systems to this area in the present-day climate (Hope et al., 2010). The analysis
focuses on a smaller south-west box rather than the larger southern Australia domain as there is a larger increase in
precipitation in the LGM evident in the south-west region in many models. This region is also climatically distinct in the
modern climate, experiencing higher winter rainfall than surrounding areas, with a recent strong drying trend (Hope et al.
410   2010).

Figure 11 shows the relationship between the JJA LGM change in precipitation averaged over south-west Australia
(30ºS-35ºS, 115ºE-120ºE; see Figure 2) and the change in strength of the westerly winds over the same latitude range, but
with a wider longitude range for the entire Southern Australian region (110°E-155°E). The Pearson correlation coefficient
between the two variables is r = 0.55, and the corresponding p-value is 0.082, indicating a moderate positive correlation
415   between the two variables. This suggests that larger westerly wind speeds are likely to be associated with enhanced
precipitation in this region. The wind and temperature anomaly values for each model are listed in Table S1 in the
Supplement.

Sime et al. (2013) proposed that there is no clear relationship between the displacements of westerlies and enhanced
precipitation at the LGM based on PMIP models. While we also find no clear relationship over the SH or Southern Australia
420   scale, over the south-west Australian corner we do find a moderate correlation between westerly wind strength and
precipitation changes over south-west Australia at the LGM.
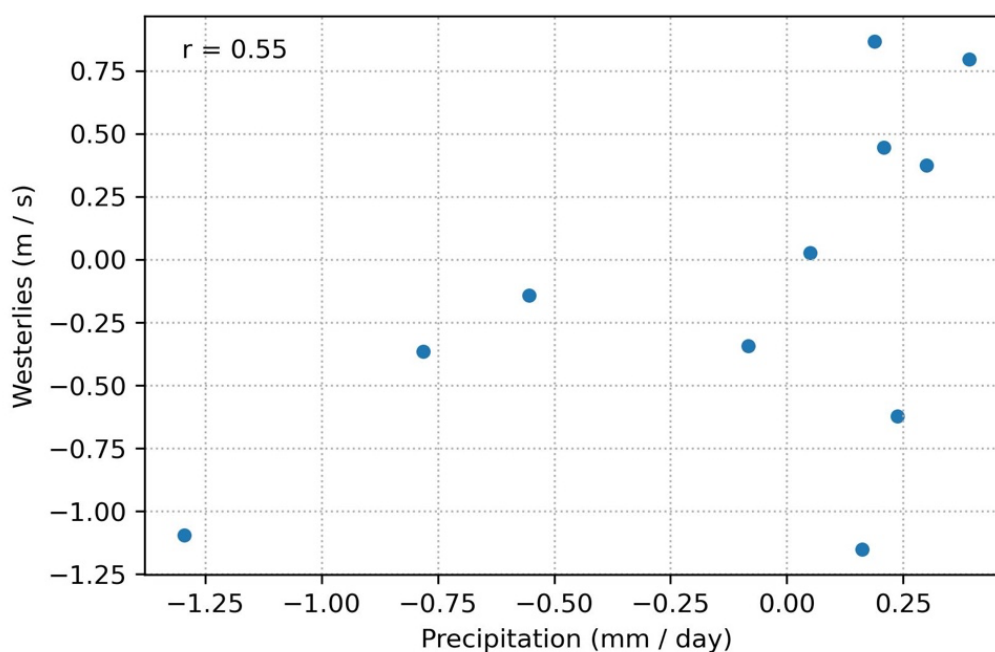
425

Figure 11: Relationship between JJA LGM - PI anomalies for the strengths of the 850 hPa westerlies over 30ºS to 35ºS Southern Australia domain and precipitation averages over smaller south-west Australia domain (30ºS-35ºS, 115ºE-120ºE) simulated by CMIP5 and CMIP6 models (excluding CMIP6 INM-CM4-8 model).

4 Discussion and Conclusions

430 This study has evaluated the temperature, precipitation and wind changes over the Australian region at the LGM compared to pre-industrial conditions based on CMIP5 and CMIP6 model simulations. We now summarise the key finding from the model simulations and briefly compare these with published proxy records of LGM temperature, precipitation and atmospheric circulation from this region, introduced in Section 1.

4.1 Temperature

435 The models simulate regional cooling of annual surface temperatures in the range of -1.8 ºC to -4.0 ºC (MMM = -2.6 ºC) in the Australian domain (0-45°S, 110°E-160°E), with larger cooling over land and particularly over coastal regions with expanded land area at the LGM. On seasonal time scales, cooling is slightly larger in MAM and JJA over this region. Our model results for temperature change generally agree well with available proxy records and previous modelling studies although there are some LGM proxy records which do not show good agreements with the models. For example, Miller et al.

440 (1997) and Hope (2009) reconstructed greater cooling over land than was simulated by the models, with Miller et al. (1997) finding cooling of 9 ºC in inland Australia and Hope (2009) finding cooling of 4-6 ºC in the New Guinea highlands. This may be due to uncertainties in the proxy reconstruction. Alternatively, the models may not be simulating the extent of cooling over land in the LGM simulations. In the case of proxy records over high topography (e.g. Hope, 2009), the models may also not resolved the details of the topography and associated cooling.

445 We also tested whether using surface air temperature ("tas") from models provided a better match with proxy records than using surface temperature ("ts") which is the land and ocean surface temperature. Seasonal comparison with LGM temperature anomalies based on these two variables (see Supplementary Figure S8) indicates that surface air temperature does not provide greater agreement with the extent of LGM cooling seen in proxy records.

4.2 Precipitation

450 The models simulate an overall reduced precipitation over the Australian region, with negative annual average anomalies in the majority of models and the MMM. Seasonal MMM precipitation anomalies (Figure 8) indicate widespread, slightly lower precipitation than today, except for slightly higher precipitation during DJF, in the north-eastern central Northern Australia, northern Cape York, and all of Tasmania except the west coast; during JJA in SW WA; and during SON in the subtropical eastern margin of the continent. P-E patterns (Figure 10) do not show obviously intensified wetness of any
455 of the higher precipitation regions. In turn, the central Northern Australia moistening seems less clear in P-E than in P. However, overall, most of the continent experienced negative precipitation and positive P-E anomalies, implying that most regions would have experienced LGM hydroclimatic stasis (i.e. little change in moisture availability) or slightly wetter conditions, particularly on seasonal time scales.

Some paleoclimate proxies (e.g. Fitzsimmons et al., 2013; Petherick et al., 2013; Cadd et al., 2018) have been
460 interpreted as indicating substantially lower LGM moisture availability, which is not consistent with the changes in P-E from the PMIP/CMIP simulations analysed in this study. On the other hand, studies of paleo-river channels in the Murray-Darling Basin indicate that relatively high fluvial discharge, and thus moisture availability, were maintained at the LGM (Kemp et al., 2017; Hesse et al., 2018). The contradiction between some proxy reconstructions and model simulations may partly reflect the fact that vegetation-based hydroclimate reconstructions have not taken into account the effects of low CO_2 on
465 plant growth (Prentice et al., 2017; Sniderman et al., 2019).

4.3 Winds

Similar to many other studies, this study did not find a consistent equatorward or poleward shift in the SH mid-latitude westerly winds at the LGM based on the available CMIP5 and CMIP6 model simulations. Focusing on the Australian sector, this study tried to detect changes in the latitude of the SH westerly winds in austral winter (JJA) through investigating the
470 position of the boundary lines between westerly and easterly winds for each model. From our calculations of their latitudinal positions at the LGM and PI, most models agree on an equatorward shift at the LGM with a multi-model average

displacement of 0.65º northwards. However, we did not identify a consistent shift in maximum SH mid-latitude zonal winds in the LGM simulations. Future work could conduct additional evaluations such as examining upper-level winds (as in Kageyama et al., 2021), or use a larger ensemble of models and more comprehensive dynamical analysis to address this

475   question.

4.4 Conclusions

This research presents an initial evaluation and analysis for the climate conditions (temperature, precipitation, wind) over a wider Australian domain (including adjacent regions of Indonesia and New Guinea) at the LGM using the ensemble of twelve CMIP5 and CMIP6 models with available PMIP LGM simulations. Previously, few studies using coupled model

480   simulations of LGM climate have focused on this region or even the Southern Hemisphere. The results offer insights into some regional Australian climate variations during the LGM, and the inter-connections between climate variables in different seasons. Our model results generally agree with published proxy records and other model studies, with some exceptions as discussed in Section 4.

Several analyses were also conducted in this study to assess the relationships between westerly winds and

485   precipitation, and temperature and precipitation. A moderate positive correlation between the JJA westerlies and precipitation over south-west Australia (30ºS-35ºS) was found, indicating larger westerly wind speeds with enhanced precipitation. In contrast, no clear relationship between surface temperature and precipitation changes is found in this study, which leaves future work to further investigate drivers of regional LGM precipitation change.

Code and data availability

490   The CMIP5 and CMIP6 model data used in this study are available from the Earth System Grid Federation.

Supplement

The Supplement related to this article is available online at:

Author contributions

YD and JRB designed the study. YD carried out the data analysis and led the writing of the manuscript. JRB and JMKS

495   provided comments on the results and contributed to the writing of the manuscript.

Competing interests

The authors declare that they have no conflict of interest.

Acknowledgments

Josephine R. Brown and Yanxuan Du acknowledge support from the Australian Research Council Centre of Excellence for
Climate Extremes (CE170100023). We acknowledge the World Climate Research Programme, which, through its Working
Group on Coupled Modelling, coordinated and promoted CMIP6. We thank the climate modelling groups for producing and
making available their model output, the Earth System Grid Federation (ESGF) for archiving the data and providing access,
and the multiple funding agencies who support CMIP6 and ESGF. CMIP5 and CMIP6 model outputs were made available
with the assistance of resources from the National Computational Infrastructure (NCI), which is supported by the Australian
government.

References

Adloff, M., Reick, C. H., and Claussen, M.: Earth system model simulations show different feedback strengths of the
terrestrial carbon cycle under glacial and interglacial conditions, Earth Syst. Dynam., 9, 413–425,
https://doi.org/10.5194/esd-9-413- 2018, 2018.

Annan, J. D. and Hargreaves, J. C.: A new global reconstruction of temperature changes at the Last Glacial Maximum, Clim.
Past, 9, 367–376, https://doi.org/10.5194/cp-9-367-2013, 2013.

Annan, J. D., Hargreaves, J. C., and Mauritsen, T.: A new global surface temperature reconstruction for the Last Glacial
Maximum, Clim. Past, 18, 1883–1896, https://doi.org/10.5194/cp-18-1883-2022, 2022.

Braconnot, P., Harrison, S. P., Kageyama, M., Bartlein, P. J., Masson-Delmotte, V., Abe-Ouchi, A., Otto-Bliesner, B., and
Zhao, Y.: Evaluation of climate models using palaeoclimatic data, Nat. Clim. Change, 2, 417-424,
https://doi.org/10.1038/nclimate1456, 2012.

Brady, E. C., Otto-Bliesner, B. L., Kay, J. E., and Rosenbloom, N.: Sensitivity to Glacial Forcing in the CCSM4, J. Climate,
26, 1901–1925, https://doi.org/10.1175/JCLI-D-11-00416.1, 2013.

Brown, J. R., Brierley, C. M., An, S. I., Guarino, M. V., Stevenson, S., Williams, C. J. R., Zhang, Q., Zhao, A., Abe-Ouchi,
525 A., Braconnot, P., Brady, E. C., Chandan, D., D'Agostino, R., Guo, C., LeGrande, A. N., Lohmann, G., Morozova, P. A.,
Ohgaito, R., O' ishi, R., Otto-Bliesner, B. L., Peltier, W. R., Shi, X., Sime, L., Volodin, E. M., Zhang, Z., and Zheng, W.:
Comparison of past and future simulations of ENSO in CMIP5/PMIP3 and CMIP6/PMIP4 models, Clim. Past, 16, 1777-
1805, https://doi.org/10.5194/cp-16-1777-2020, 2020.

530 Cadd, H. R., Tibby, J., Barr, C., Tyler, J., Unger, L., Leng, M. J., Marshall, J. C., McGregor, G., Lewis, R., Arnold, L. J.,
Lewis, T., and Baldock, J.: Development of a southern hemisphere subtropical wetland (Welsby Lagoon, south-east
Queensland, Australia) through the last glacial cycle, Quaternary Sci. Rev., 202, 53-65,
https://doi.org/10.1016/j.quascirev.2018.09.010, 2018.

535 Cadd, H., Petherick, L., Tyler, J., Herbert, A., Cohen, T., Sniderman, K., Barrows, T. T., Fulop, R. T., Knight, J., Kershaw,
A. P., Colhoun, E. A., and Harris, M.: A continental perspective on the timing of environmental change during the last
glacial stage in Australia, Quaternary Res., 102, 5-23, https://doi.org/10.1017/qua.2021.16, 2021.

Chadwick, R., Boutle, I., & Martin, G.: Spatial patterns of precipitation change in CMIP5: Why the rich do not get richer in
540 the tropics, J. Climate, 26, 3803-3822, https://doi.org/10.1175/JCLI-D-12-00543.1, 2013.

Chavaillaz, Y., Codron, F., & Kageyama, M.: Southern westerlies in LGM and future (RCP4.5) climates, Clim. Past, 9, 517-
524, https://doi.org/10.5194/cp-9-517-2013, 2013.

545 Clark, P. U., Dyke, A. S., Shakun, J. D., Carlson, A. E., Clark, J., Wohlfarth, B., Mitrovica, J. X., Hostetler, S. W., and
McCabe, A. M.: The Last Glacial Maximum, Science, 325, 710–714, https://doi.org/10.1126/science.1172873, 2009.

Clarkson, C., Jacobs, Z., Marwick, B., Fullagar, R., Wallis, L., Smith, M., Roberts, R. G., Hayes, E., Lowe, K., Carah, X.,
Florin, S. A., McNeil, J., Cox, D., Arnold, L. J., Hua, Q., Huntley, J., Brand, H. E. A., Manne, T., Fairbairn, A., Shulmeister,
550 J., Lyle, L., Salinas, M., Page, M., Connell, K., Park, G., Norman, K., Murphy, T., and Pardoe, C.: Human occupation of
northern Australia by 65,000 years ago, Nature, 547, 306, https://doi.org/10.1038/nature22968, 2017.

Cohen, T.J., John D. Jansen, Luke A. Gliganic, Joshua R. Larsen, Gerald C. Nanson, Jan-Hendrik May, Brian G. Jones,
David M. Price; Hydrological transformation coincided with megafaunal extinction in central Australia. Geology 43 (3):
555 195–198. doi: https://doi.org/10.1130/G36346.1, 2015.

Danabasoglu, G., Lamarque, J.-F., Bacmeister, J., Bailey, D. A., DuVivier, A. K., Edwards, J., Emmons, L. K., Fasullo, J., Garcia, R., Gettelman, A., Hannay, C., Holland, M. M., Large, W. G., Lauritzen, P. H., Lawrence, D. M., Lenaerts, J. T. M., Lindsay, K., Lipscomb, W. H., Mills, M. J., Neale, R., Oleson, K. W., Otto-Bliesner, B., Phillips, A. S., Sacks, W., Tilmes,

560   S., van Kampenhout, L., Vertenstein, M., Bertini, A., Dennis, J., Deser, C., Fischer, C., Fox-Kemper, B., Kay, J. E., Kinnison, D., Kushner, P. J., Larson, V. E., Long, M. C., Mickelson, S., Moore, J. K., Nienhouse, E., Polvani, L., Rasch, P. J., and Strand, W. G.: The Community Earth System Model Version 2 (CESM2), J. Adv. Model. Earth Syst., 12, e2019MS001916, https://doi.org/10.1029/2019MS001916, 2020.

565   Denniston, R. F., Asmerom, Y., Lachniet, M., Polyak, V. J., Hope, P., An, N., Rodzinyak, K., and Humphreys, W. F.: A Last Glacial Maximum through middle Holocene stalagmite record of coastal Western Australia climate, Quaternary Sci. Rev., 77, 101-112, https://doi.org/10.1016/j.quascirev.2013.07.002, 2013.

De Deckker, P., Moros, M., Perner, K., Blanz, T., Wacker, L., Schneider, R., Barrows, T. T., O' Loingsign, T., and Jansen,

570   E.: Climatic evolution in the Australian region over the last 94 ka - spanning human occupancy -, and unveiling the Last Glacial Maximum, Quaternary Sci. Rev., 249, https://doi.org/10.1016/j.quascirev.2020.106593, 2020.

DiNezio, P. N., and Tierney, J. E.: The effect of sea level on glacial Indo-Pacific climate, Nat. Geosci., 6, 485-491, https://doi.org/10.1038/NGEO1823, 2013.

575

Dufresne, J. L., Foujols, M. A., Denvil, S., Caubel, A., Marti, O., Aumont, O., Balkanski, Y., Bekki, S., Bellenger, H., Benshila, R., Bony, S., Bopp, L., Braconnot, P., Brockmann, P., Cadule, P., Cheruy, F., Codron, F., Cozic, A., Cugnet, D., de, Noblet, N., Duvel, J. P., Ethé, C., Fairhead, L., Fichefet, T., Flavoni, S., Friedlingstein, P., Grandpeix, J. Y., Guez, L., Guilyardi, E., Hauglustaine, D., Hourdin, F., Idelkadi, A., Ghattas, J., Joussaume, S., Kageyama, M., Krinner, G.,

580   Labetoulle, S., Lahellec, A., Lefebvre, M. P., Lefevre, F., Levy, C., Li, Z. X., Lloyd, J., Lott, F., Madec, G., Mancip, M., Marchand, M., Masson, S., Meurdesoif, Y., Mignot, J., Musat, I., Parouty, S., Polcher, J., Rio, C., Schulz, M., Swingedouw, D., Szopa, S., Talandier, C., Terray, P., Viovy, N., and Vuichard, N.: Climate change projections using the IPSL-CM5 Earth System Model: from CMIP3 to CMIP5, Clim. Dynam., 40, 2123–2165, https://doi.org/10.1007/s00382-012-1636-1, 2013.

585   Ehlers, J., and Gibbard, P. L.: The extent and chronology of Cenozoic Global Glaciation, Quat. Int., 164-165, 6-20, https://doi.org/10.1016/j.quaint.2006.10.008, 2007.

Eyring, V., Bony, S., Meehl, G. A., Senior, C. A., Stevens, B., Stouffer, R. J., and Taylor, K. E.: Overview of the Coupled Model Intercomparison Project Phase 6 (CMIP6) experimental design and organization, Geosci. Model Dev., 9, 1937–1958,

590   https://doi.org/10.5194/gmd-9-1937-2016, 2016.

Fitzsimmons, K. E., Cohen, T. J., Hesse, P. P., Jansen, J., Nanson, G. C., May, J.-H., Barrows, T. T., Haberlah, D., Hilgers, A., Kelly, T., Larsen, J., Lomax, J., and Treble, P.: Late Quaternary palaeoenvironmental change in the Australian drylands, Quaternary Sci. Rev., 74, 78-96, https://doi.org/10.1016/j.quascirev.2012.09.007, 2013.

595

Fitzsimmons, K. E., Miller, G. H., Spooner, N. A., & Magee, J. W.: Aridity in the monsoon zone as indicated by desert dune formation in the Gregory Lakes basin, northwestern Australia, Aust. J. Earth Sci., 59, 469-478, https://doi.org/10.1080/08120099.2012.686171, 2012.

600   Hajima, T., Watanabe, M., Yamamoto, A., Tatebe, H., Noguchi, M. A., Abe, M., Ohgaito, R., Ito, A., Yamazaki, D., Okajima, H., Ito, A., Takata, K., Ogochi, K., Watanabe, S., and Kawamiya, M.: Development of the MIROC-ES2L Earth system model and the evaluation of biogeochemical processes and feedbacks, Geosci. Model Dev., 13, 2197–2244, https://doi.org/10.5194/gmd-13- 2197-2020, 2020.

605   Hesse, P. P., Williams, R., Ralph, T. J., Frirs, K. A., Larkin, Z. T., Westaway, K. E., and Farebrother, W.: Palaeohydrology of lowland rivers in the Murray-Darling Basin, Australia, Quaternary Sci. Rev., 200, 85-105, https://doi.org/10.1016/j.quascirev.2018.09.035, 2018.

Holden, P. B., Edwards, N. R., Oliver, K. I. C., Lenton, T. M., and Wilkinson, R. D.: A probabilistic calibration of climate
610   sensitivity and terrestrial carbon change in GENIE-1, Clim. Dynam., 35, 785, https://doi.org/10.1007/s00382-009-0630-8, 2010.

Hope, G.: Environmental change and fire in the Owen Stanley Ranges, Papua New Guinea, Quaternary Sci. Rev., 28, 2261-2276, https://doi.org/10.1016/j.quascirev.2009.04.012, 2009.

615

Hope, P: The Weather and Climate of Australia at the Last Glacial Maximum, PhD Thesis, University of Melbourne, School of Earth Sciences, 2005.

Hope, P., Timbal, B., and Fawcett, R.: Associations between rainfall variability in the southwest and southeast of Australia
620   and their evolution through time, Int. J. Climatol., 30, 1360-1371, https://doi.org/10.1002/joc.1964, 2010.

Hughes, P. D., Gibbard, P. L., and Ehlers, J.: Timing of glaciation during the last glacial cycle: evaluating the concept of a global 'Last Glacial Maximum' (LGM), Earth-Sci Rev., 125, 198–171, https://doi.org/10.1016/j.earscirev.2013.07.003, 2013.

625

Jungclaus, J., Mikolajewicz, U., Kapsch, M.-L., D'Agostino, R., Wieners, K.-H., Giorgetta, M., Reick, C., Esch, M., Bittner, M., Legutke, S., Schupfner, M., Wachsmann, F., Gayler, V., Haak, H., de Vrese, P., Raddatz, T., Mauritsen, T., von Storch, J.-S., Behrens, J., Brovkin, V., Claussen, M., Crueger, T., Fast, I., Fiedler, S., Hagemann, S., Hohenegger, C., Jahns, T., Kloster, S., Kinne, S., Lasslop, G., Kornblueh, L., Marotzke, J., Matei, D., Meraner, K., Modali, K., Müller, W., Nabel, J., Notz, D., Peters, K., Pincus, R., Pohlmann, H., Pongratz, J., Rast, S., Schmidt, H., Schnur, R., Schulzweida, U., Six, K., Stevens, B., Voigt, A., and Roeckner, E.: MPI-M MPI-ESM1.2-LR model output prepared for CMIP6 PMIP lgm, Version 20190710, Earth System Grid Federation, https://doi.org/10.22033/ESGF/CMIP6.6642, 2019.

Kageyama, M., Albani, S., Braconnot, P., Harrison, S. P., Hopcroft, P. O., Ivanovic, R. F., Lambert, F., Marti, O., Peltier, W. R., Peterschmitt, J.-Y., Roche, D. M., Tarasov, L., Xu Zhang, Brady, E. C., Haywood, A. M., LeGrande, A. N., Lunt, D. J., Mahowald, N. M., Mikolajewicz, U., & Nisancioglu, K. H.: The PMIP4 contribution to CMIP6 - Part 4: Scientific objectives and experimental design of the PMIP4-CMIP6 Last Glacial Maximum experiments and PMIP4 sensitivity experiments, Geosci. Model Dev., 10, 4035–4055, https://doi.org/10.5194/gmd-10-4035-2017, 2017.

Kageyama, M., Braconnot, P., Harrison, S. P., Haywood, A. M., Jungclaus, J. H., Otto-Bliesner, B. L., Peterschmitt, J.-Y., Abe-Ouchi, A., Albani, S., Bartlein, P. J., Brierley, C., Crucifix, M., Dolan, A., Fernandez-Donado, L., Fischer, H., Hopcroft, P. O., Ivanovic, R. F., Lambert, F., Lunt, D. J., Mahowald, N. M., Peltier, W. R., Phipps, S. J., Roche, D. M., Schmidt, G. A., Tarasov, L., Valdes, P. J., Zhang, Q., and Zhou, T.: The PMIP4 contribution to CMIP6 – Part 1: Overview and over-arching analysis plan, Geosci. Model Dev., 11, 1033–1057, https://doi.org/10.5194/gmd-11-1033-2018, 2018.

Kageyama, M., Harrison, S. P., Kapsch, M.-L., Lofverstrom, M., Lora, J. M., Mikolajewicz, U., Sherriff-Tadano, S., Vadsaria, T., Abe-Ouchi, A., Bouttes, N., Chandan, D., Gregoire, L. J., Ivanovic, R. F., Izumi, K., LeGrande, A. N., Lhardy, F., Lohmann, G., Morozova, P. A., Ohgaito, R., Paul, A., Peltier, W. R., Poulsen, C. J., Quiquet, A., Roche, D. M., Shi, X., Tierney, J. E., Valdes, P. J., Volodin, E., and Zhu, J.: The PMIP4 Last Glacial Maximum experiments: preliminary results and comparison with the PMIP3 simulations, Clim. Past, 17, 1065–1089, https://doi.org/10.5194/cp-17-1065-2021, 2021.

Kemp, J., Pietsch, T., Gontz, A., and Olley, J: Lacustrine-fluvial interactions in Australia's Riverine Plains, Quaternar Sci. Rev., 166, 352-362, https://doi.org/10.1016/j.quascirev.2017.02.015, 2017.

Kim, S. J., Flato, G., and Boer, G.: A coupled climate model simulation of the Last Glacial Maximum, Part 2: approach to equilibrium, Clim. Dynam., 20, 635-661, https://doi.org/10.1007/s00382-002-0292-2, 2003.

Kitoh, A., Murakami, S., and Koide, H.: A simulation of the Last Glacial Maximum with a coupled atmosphere-ocean GCM, 28, 2221-2224, https://doi.org/10.1029/2000GL012271, 2001.

660

Kohfeld, K. E., Graham, R. M., de Boer, A. M., Sime, L. C., Wolff, E. W., Le Quéré, C., and Bopp, L.: Southern Hemisphere westerly wind changes during the Last Glacial Maximum: paleo-data synthesis, Quaternary Sci. Rev., 68, 76-95, https://doi.org/10.1016/j.quascirev.2013.01.017, 2013.

665 Lambeck, K., Rouby, H., Purcell, A., Sun, Y., and Sambridge, M.: Sea level and global ice volumes from the Last Glacial Maximum to the Holocene, Proc. Natl. Acad. Sci. U.S.A., 111, 15296–15303, https://doi.org/10.1073/pnas.1411762111, 2014.

Lamy, F., Gersonde, R., Winckler, G., Esper, O., Jaeschke, A., Kuhn, G., Ullermann, J., Martinez-Garcia, A., Lambert, F., 670 and Kilian, R.: Increased Dust Deposition in the Pacific Southern Ocean During Glacial Periods, Science, 343, 404–407, https://doi.org/10.1126/science.l245424, 2014.

Liu, Z., Lu, Z., Wen, X., Otto-Bliesner, B. L., Timmermann, A., and Cobb, K. M.: Evolution and forcing mechanisms of El Niño over the past 21,000 years, Nature, 515, 550-553, https://doi.org/10.1038/nature13963, 2014.

675

Liu, S., Jiang, D., and Lang, X.: The Weakening and Eastward Movement of ENSO Impacts during the Last Glacial Maximum, J. Climate, 33, 5507-5526, https://doi.org/10.1175/JCLI-D-19-0728.1, 2020.

Miller, G. H., Magee, J. W., and Jull, A. J. T.: Low-latitude glacial cooling in the Southern Hemisphere from amino-acid 680 racemization in emu eggshells, Nature, 385, 241-244, https://doi.org/10.1038/385241a0, 1997.

Newnham, R. M., Lowe, D. J., Giles, T., and Alloway, B. V.: Vegetation and climate of Auckland, New Zealand, since ca. 32 000 cal. yr ago: Support for an extended LGM, J. Quat. Sci., 22, 517–534, https://doi.org/10.1002/jqs.1137, 2007.

685 Ohgaito, R., Yamamoto, A., Hajima, T., O'ishi, R., Abe, M., Tatebe, H., Abe-Ouchi, A., and Kawamiya, M.: PMIP4 experiments us- ing MIROC-ES2L Earth system model, Geosci. Model Dev., 14, 1195–1217, https://doi.org/10.5194/gmd-14-1195-2021, 2021.

Otto-Bliesner, B. L., Brady, E. C., Clauzet, G., Tomas, R., Levis, S., and Kothavala, Z.: Last Glacial Maximum and 690 Holocene Climate in CCSM3, J. Climate, 9, 2526-2544, https://doi.org/10.1175/JCLI3748.1, 2006.

Petherick, L., Bostock, H., Cohen, T. J., Fitzsimmons, K., Tibby, J., Fletcher, M. S., Moss, P., Reeves, J., Monney, S., Barrows, T., Kemp, J., Jansen, J., Nanson, G., and Dosseto, A.: Climatic records over the past 30 ka from temperate Australia – a synthesis from the Oz-INTIMATE workgroup, Quaternary Sci. Rev., 74, 58-77,
695 https://doi.org/10.1016/j.quascirev.2012.12.012, 2013.

Prentice, I. C., Cleator, S. F., Huang, Y. H., Harrison, S. P., and Roulstone, I.: Reconstructing ice-age palaeoclimates: Quantifying low-CO2 effects on plants, Glob. Planet. Change., 149, 166–176, https://doi.org/10.1016/j.gloplacha.2016.12.012, 2017.

700

Prentice, I. C., Villegas-Diaz, R., and Harrison, S. P.: Accounting for atmospheric carbon dioxide variations in pollen-based reconstruction of past hydroclimates, Glob. Planet. Change., 211, https://doi.org/10.1016/j.gloplacha.2022.103790, 2022.

Reeves, J. M., Bostock, H. C., Ayliffe, L. K., Barrows, T. T., De Deckker, P., Devriendt, L. S., Dunbar, G. B., Drysdale, R.
705 N., Fitzsimmons, K. E., Gagan, M. K., Griffiths, M. L., Haberle, S. G., Jansen, J. D., Krause, C., Lewis, S., McGregor, H. V., Mooney, S. D., Moss, P., Nanson, G. C., Purcell, A., and van der Kaars, S.: Palaeoenvironmental change in tropical Australasia over the last 30,000 years - a synthesis by the OZ-INTIMATE group, Quaternary Sci. Rev., 74, 97-114, https://doi.org/10.1016/j.quascirev.2012.11.027, 2013a.

710 Reeves, J. M., Barrows, T. T., Cohen, T. J., Kiem, A. S., Bostock, H. C., Fitzsimmons, K. E., Jansen, J. D., Kemp, J., Krause, C., Petherick, L., and Phipps, S. J.: Climate variability over the last 35,000 years recorded in marine and terrestrial archives in the Australian region: an OZ-INTIMATE compilation, Quaternary Sci. Rev., 74, 21-34, https://doi.org/10.1016/j.quascirev.2013.01.001, 2013b.

715 Renoult, M., Annan, J. D., Hargreaves, J. C., Sagoo, N., Flynn, C., Kapsch, M.-L., Li, Q., Lohmann, G., Mikolajewicz, U., Ohgaito, R., Shi, X., Zhang, Q., and Mauritsen, T.: A Bayesian framework for emergent constraints: case studies of climate sensitivity with PMIP, Clim. Past, 16, 1715–1735, https://doi.org/10.5194/cp-16- 1715-2020, 2020.

Roderick, M. L., Farquhar, G. D., and Greve, P.: On the assessment of aridity with changes in atmospheric CO_2, Water
720 Resour. Res., 51, 5450–5463, https://doi.org/10.1002/2015WR017031, 2015.

Rojas, M.: Sensitivity of Southern Hemisphere circulation to LGM and 4 × CO2 climates, Geophys. Res. Lett., 40, 965-970, https://doi.org/10.1002/grl.50195, 2013.

725 Rojas, M., Moreno, P., Kageyama, M., Crucifix, M., Hewitt, C., Abe-Ouchi, A., Ohgaito, R., Brady, E. C., and Hope, P.: Southern Westerlies during the last glacial maximum in PMIP2 simulations, Clim. Dynam., 32, 525–548, https://doi.org/10.1007/s00382-008-0421-7, 2009.

Rowe, C., Wurster, C., Zwart, C., Brand, M., Hutley, L., Levchenko, V., and Bird, M.: Vegetation over the last glacial
730 maximum at Girraween Lagoon, monsoonal northern Australia, Quaternary Res., 102, 39-52, https://doi.org/10.1017/qua.2020.50, 2021.

Scheff, J., Seager, R., Liu, H., and Coats, S.: Are Glacials Dry? Consequences for Paleoclimatology and for Greenhouse Warming, J. Climate, 30, 6593-6609, https://doi.org/10.1175/JCLI-D-16-0854.1, 2017.

735

Schneider von Deimling, T., Held, H., Ganopolski, A., and Rahmstorf, S.: Climate sensitivity estimated from ensemble simulations of glacial climate, Clim. Dynam., 27, 149-163, https://doi.org/10.1007/s00382-006-0126-8, 2006.

Seltzer, A. M., Ng, J., Aeschbach, W., Kipfer, R., Kulongoski, J. T., Severinghaus, J. P., and Stute, M.: Widespread six
740 degrees Celsius cooling on land during the Last Glacial Maximum, Nature, 593, 228–232, https://doi.org/10.1038/s41586-021-03467-6, 2021.

Sidorenko, D., Rackow, T., Jung, T., Semmler, T., Barbi, D., Danilov, S., Dethloff, K., Dorn, W., Fieg, K., Goßling, H. F., Handorf, D., Harig, S., Hiller, W., Juricke, S., Losch, M., Schröter, J., Sein, D. V., and Wang, Q.: Towards multi-resolution
745 global climate modeling with ECHAM6-FESOM, Part I: model formulation and mean climate, Clim. Dynam., 44, 757–780, https://doi.org/10.1007/s00382-014-2290-6, 2015.

Sime, L. C., Kohfeld, K. E., Le Quéré, C., Wolff, E. W., de Boer, A. M., Graham, R. M., and Bopp, L.: Southern Hemisphere westerly wind changes during the Last Glacial Maximum: model-data comparison, Quaternary Sci. Rev., 64,
750 104-120, https://doi.org/10.1016/j.quascirev.2012.12.008, 2013.

Sniderman, J. M. K., Hellstrom, J., Woodhead, J. D., Drysdale, R. N., Bajo, P., Archer, M., and Hatcher, L.: Vegetation and climate change in southwestern Australia during the Last Glacial Maximum, Geophys. Res. Lett., 46, 1709–1720, https://doi.org/10.1029/2018GL080832, 2019.

755

Sueyoshi, T., Ohgaito, R., Yamamoto, A., Chikamoto, M. O., Hajima, T., Okajima, H., Yoshimori, M., Abe, M., O'ishi, R., Saito, F., Watanabe, S., Kawamiya, M., and Abe-Ouchi, A.: Set-up of the PMIP3 paleoclimate experiments conducted using an Earth system model, MIROC-ESM, Geosci. Model Dev., 6, 819–836, https://doi.org/10.5194/gmd-6-819-2013, 2013.

760 Taylor, K. E., Stouffer, R. J., and Meehl, G. A.: An Overview of CMIP5 and the Experiment Design, Bull. Amer. Meteor., 93, 485–498, https://doi.org/10.1175/BAMS-D-11-00094.1, 2012.

Tierney, J. E., Zhu, J., King, J., Malevich, S. B., Hakim, G. J., and Poulsen, C. J.: Glacial cooling and climate sensitivity revisited, Nature, 584, 569-573, https://doi.org/10.1038/s41586-020-2617-x, 2020a.

765

Tierney, J. E., Poulsen, C. J., Montanez, I. P., Bhattacharya, T., Feng, R., Ford, H. L., Hönisch, B., Inglis, G. N., Petersen, S. V., Sagoo, N., Tabor, C. R., Thirumalai, K., Zhu, J., Burls, N. J., Foster, G. L., Goddéris, Y., Huber, B. T., Ivany, L. C., Turner, S. K., Lunt, D. J., McElwain, J. C., Mills, B. J. W., Otto-Bliesner, B. L., Ridgwell, A., and Zhang, Y. G.: Past climates inform our future, Science, 370, eaay3701, https://doi.org/10.1126/science.aay3701, 2020b.

770

Treble, P. C., Baker, A., Ayliffe, L. K., Cohen, T. J., Hellstrom, J. C., Gagan, M. K., Frisia, S., Drysdale, R. N., Griffiths, A. D., and Borsato, A.: Hydroclimate of the Last Glacial Maximum and deglaciation in southern Australia's arid margin interpreted from speleothem records (23–15 ka), Clim. Past, 13, 667-687, https://doi.org/10.5194/cp-13-667-2017, 2017.

775 Ullman, D. J., LeGrande, A. N., Carlson, A. E., Anslow, F. S., and Licciardi, J. M.: Assessing the impact of Laurentide Ice Sheet topography on glacial climate, Clim. Past, 10, 487–507, https://doi.org/10.5194/cp-10-487-2014, 2014.

Ujvari, G., Wegner, W., Klotzli, U., Horschinegg, M., and Hippler, D.: Sr-Nd-Hf Isotopic Analysis of < 10 mg Dust Samples: Implications for Ice Core Dust Source Fingerprinting, Geochem. Geophys., 19, 60–63, 780 https://doi.org/10.1002/2017GC007136, 2018.

Voldoire, A., Sanchez-Gomez, E., Salas y Mélia, D., Decharme, B., Cassou, C., Sénési, S., Valcke, S., Beau, I., Alias, A. Chevallier, M., Déqué, M., Deshayes, J., Douville, H., Fernan- dez, E., Madec, G., Maisonnave , E., Moine, M.-P., Planton, S., Saint-Martin, D., Szopa, S., Tyteca, S., Alkama, R., Bela- mari, S., Braun, A., Coquart, L., and Chauvin, F.: The CNRM-785 CM5.1 global climate model: description and basic evaluation, Clim. Dynam., 40, 2091–2121, https://doi.org/10.1007/s00382- 011-1259-y, 2013.

Volodin, E., Mortikov, E., Kostrykin, S., Galin, V., Lykossov, V., Gritsun, A., Diansky, N., Gusev, A., Iakovlev, N., Shestakova, A., and Emelina, S.: Simulation of the modern climate us- ing the INM-CM48 climate model, Russian Journal 790 of Nu- merical Analysis and Mathematical Modelling, 33, 367–374, https://doi.org/10.1515/rnam-2018-0032, 2018.

Yan, M., Wang, B., Liu, J., Zhu, A., Ning, L., and Cao, J.: Understanding the Australian Monsoon change during the Last Glacial Maximum with a multi-model ensemble, Clim. Past, 14, 2037–2052, https://doi.org/10.5194/cp-14-2037-2018, 2018.

795   Yokoyama, Y., Esat, T. M., Thompson, W. G., Thomas, A. L., Webster, J. M., Miyairi, Y., Sawada, C., Aze, T., Matsuzaki, H., Okuno, J., Fallon, S., Braga, J.-C., Humblet, M., Iryu, Y., Potts, D. C., Fujita, K., Suzuki, A., and Kan, H.: Rapid glaciation and a two-step sea level plunge into the Last Glacial Maximum, Nature, 559, 603, https://doi.org/10.1038/s41586-018-0335-4, 2018.

800   Yukimoto, S., Adachi, Y., Hosaka, M., Sakami, T., Yoshimura, H., Hirabara, M., Tanaka, T., Shindo, E., Tsujino, H., Deushi, M., Mizuta, R., Yabu, S., Obata, A., Nakano, H., Koshiro, T., Ose, T., and Kitoh, A.: MRI-CGCM3 model output prepared for CMIP5 lgm, served by ESGF, World Data Center for Climate (WDCC) at DKRZ, https://doi.org/10.1594/WDCC/CMIP5.MRMClg, 2015.

805   Zheng, W., and Yu, Y: Paleoclimate simulations of the mid-Holocene and last glacial maximum by FGOALS, Adv. Atmos. Sci., 30, 684–698, https://doi.org/10.1007/s00376-012-2177-6, 2013.

Zhu, J., Otto-Bliesner, B. L., Brady, E. C., Poulsen, C. J., Tierney, J. E., Lofverstrom, M., and DiNezio, P.: Assessment of equilibrium climate sensitivity of the Community Earth System Model version 2 through simulation of the Last Glacial
810   Maximum, Geophys. Res. Lett., 48, https://doi.org/10.1029/2020GL091220, 2021.